PROCEEDINGS A

royalsocietypublishing.org/journal/rspa

Research

Cite this article: Dalwadi MP, Pearce P. 2023 Universal dynamics of biological pattern formation in spatio-temporal morphogen variations. *Proc. R. Soc. A* **479**: 20220829. https://doi.org/10.1098/rspa.2022.0829

Received: 12 December 2022
Accepted: 23 February 2023

Subject Areas:
applied mathematics

Keywords:
pattern formation, Turing patterns, quorum sensing, delayed bifurcations, critical slowing down

Authors for correspondence:
Mohit P. Dalwadi
e-mail: m.dalwadi@ucl.ac.uk
Philip Pearce
e-mail: philip.pearce@ucl.ac.uk

†These authors contributed equally to this study.

Electronic supplementary material is available online at https://doi.org/10.6084/m9.figshare.c.6463359.

THE ROYAL SOCIETY PUBLISHING

Universal dynamics of biological pattern formation in spatio-temporal morphogen variations

Mohit P. Dalwadi[1,2,†] and Philip Pearce[1,2,†]

[1]Department of Mathematics, and [2]Institute for the Physics of Living Systems, University College London, London, UK

MPD, 0000-0001-5017-2116; PP, 0000-0001-5788-3826

In biological systems, chemical signals termed morphogens self-organize into patterns that are vital for many physiological processes. As observed by Turing in 1952, these patterns are in a state of continual development, and are usually transitioning from one pattern into another. How do cells robustly decode these spatio-temporal patterns into signals in the presence of confounding effects caused by unpredictable or heterogeneous environments? Here, we answer this question by developing a general theory of pattern formation in spatio-temporal variations of 'pre-pattern' morphogens, which determine gene-regulatory network parameters. Through mathematical analysis, we identify universal dynamical regimes that apply to wide classes of biological systems. We apply our theory to two paradigmatic pattern-forming systems, and predict that they are robust with respect to non-physiological morphogen variations. More broadly, our theoretical framework provides a general approach to classify the emergent dynamics of pattern-forming systems based on how the bifurcations in their governing equations are traversed.

1. Introduction

In biological pattern formation, cells interpret morphogen signals to make developmental decisions based on their location in a tissue, organ, embryo or population. Such

systems have been found to be remarkably robust to a wide range of sources of variation in morphogen signals and system components [1–3]. For example, in recent work, general principles of biological pattern-forming systems have been identified that promote robustness with respect to variations in morphogen and protein production rates [2,4], in tissue or organism size [5,6], and in gene-regulatory network architecture [7]. However, these studies have generally focused on robustness with respect to variations from cell to cell or from tissue to tissue [2]—much less is understood about how such systems respond to spatio-temporal variations in morphogen concentrations within individual cells, populations or tissues, particularly over timescales faster than or similar to growth.

Recent experimental and theoretical work has demonstrated how specific gene-regulatory network architectures convert spatio-temporal morphogen signals into a required static or dynamic response [8–16]. These morphogen signals, which have been called 'pre-pattern' morphogens, can arise as a necessary part of the developmental process [8,17,18]. However, unpredictable pre-pattern morphogen fluctuations in a system may be caused by intrinsic noise [19], growth [20], cell motility or rearrangement [21–24], biochemical reactions [25,26] or external flows [13,27–29]. These studies raise the question of how to quantify the robustness of a system's gene-regulatory network output, i.e. emergent spatio-temporal patterning, with respect to variations in its pre-pattern morphogen input over a certain timescale.

A typical approach to mathematical modelling of biological pattern formation is to use reaction–diffusion equations that capture the essential dynamics of relevant morphogens [8]. In reaction–diffusion equations, gene-regulatory networks are represented using the reaction terms, and pre-pattern morphogens can be taken into account through the associated reaction parameters [18]. Such equations display self-organization in space and time via bifurcations [30,31], which often cause switch-like transitions in the solution that may correspond to biological decisions [13] or cell-fate choices [32]. Mathematically, dynamics are typically observed to slow down near bifurcations [33]. This effect is modified with additional slow timescales when the bifurcation is crossed dynamically [34,35], and these 'delayed bifurcation' effects have previously been considered in reaction–diffusion contexts [36–38], but the implications to biological pattern formation and decision-making are not understood.

Here, we connect bifurcations in reaction–diffusion systems to robustness in biological pattern formation. Although our approach is general, we consider two specific pattern-forming systems with spatio-temporal variations in pre-pattern morphogens. Mathematically, the morphogen variations correspond to variations in the coefficients of the governing reaction–diffusion equations. We use mathematical analysis to classify and quantify the dynamic response to such variations in terms of universal solution regimes that we identify. The regimes emerge as a consequence of bifurcations in the governing equations—in corresponding biological systems, the type of bifurcation is determined by the system's gene-regulatory network. Our analysis predicts an emergent timescale *associated with bifurcations*; in the relevant solution regime, this bifurcation timescale allows the system to filter out oscillatory variations in pre-pattern morphogens that occur faster than a critical timescale. This emergent timescale is different to the classic slowed timescale near a bifurcation; in systems with spatio-temporal variations the position of the bifurcation moves around, effectively acting as a dynamic crossing of the bifurcation (see electronic supplementary material for an analysis detailing the emergence of an intermediate timescale due to the dynamic crossing of a bifurcation). Surprisingly, in the two biological examples that we study, we find that the critical timescale is a few hours shorter than physiological timescales. Overall, our analysis and simulations suggest that gene-regulatory networks in some biological systems may have been tuned for robustness: they are able to ignore variations or oscillations in morphogen concentrations that happen much faster than growth, while responding appropriately to physiological morphogen variations.

The paper contains three main parts. In the first part, we derive (§2) and analyse (§3 and appendix B) generic canonical equations, or normal forms, that capture pattern-formation dynamics for a class of continuous transitions; we focus on supercritical pitchfork and transcritical

bifurcations. In the second part, we model and analyse two specific biological systems so that they can be written in terms of the canonical results (§4 and electronic supplementary material). In the final part, we summarize our results and discuss their implications for biological pattern formation (§5 and 6). Therefore, the reader most interested in the biological applications of this study can go directly to §5.

2. Derivation of normal forms

As a reaction–diffusion system undergoes a bifurcation, its dynamics can typically be approximated by a (low-dimensional) canonical weakly nonlinear equation—a normal form—whose specific functional form depends on the type of bifurcation [33]. To perform analysis relevant to several classes of biological pattern formation that manifest via continuous transitions, in this section, we focus on deriving the appropriate normal forms for (supercritical) pitchfork and transcritical bifurcations in the presence of spatio-temporal variations. In the next section, we analyse and quantify the dynamics of these normal forms as system parameters are varied; the dynamics depend on the type of bifurcation, and in which direction the system passes through the bifurcation (either 'on-to-off' or 'off-to-on'). As will be made clear in §5, pitchfork bifurcations can be associated with activator-inhibitor systems and transcritical bifurcations with autoinduction loops; in both cases, parameter variations can be linked to specific pre-pattern morphogens.

Under weakly nonlinear conditions, the effects of spatio-temporal variations in system parameters are captured by a specific variation in the related normal form near the bifurcation. We will show that variations that may appear quasi-steady away from the bifurcation can depend on the dynamics of the crossing near the bifurcation. This dynamic effect can result in an effective robustness in the system over non-standard timescales.

To understand this effect, we first demonstrate how the appropriate normal form can emerge in general through a systematic asymptotic analysis in the 'inner region' near the bifurcation. To this end, we first consider the effect of spatio-temporal variations in the parameters of the dimensionless toy reaction–diffusion problem

$$\omega\frac{\partial A}{\partial t}=D\frac{\partial^2 A}{\partial x^2}+a+k(x,t)A-\varepsilon A^n, \tag{2.1}$$

where we have non-dimensionalized time and space over their typical scales in the spatio-temporal variation. We emphasize that while (2.1) takes a specific form, the normal forms it exhibits typify supercritical pitchfork and transcritical bifurcations in pattern forming systems generally. Moreover, the asymptotic analysis we use in this section is representative of the general methodology that can be used to derive these normal forms for specific systems of interest (as we show in §4 and electronic supplementary material).

In equation (2.1), $A(x,t)$ can be thought of as a measure of the morphogen concentration (in terms of the deviation from the non-patterned state for the mode excited over the bifurcation[1]). The parameter $D>0$ represents a strength of diffusion. The parameter $a\geq 0$ represents a measure of base production in terms of the excited mode. The imposed function $k(x,t)$ represents the net strength of self-activation in comparison to decay. When $k>0$, the net effect is self-activation, while when $k<0$ the net effect is decay. The parameter $\omega>0$ represents a measure of the frequency of k variation and $\varepsilon>0$ represents the strength of nonlinear saturation effects. The exponent $n=2$ or 3, corresponds to the canonical weakly nonlinear form of an imperfect transcritical or a (supercritical) pitchfork bifurcation, respectively, as we shall see from our analysis below. Each of these characterizes a minimal gene-regulatory motif (figure 1*a*). The case with $n=2$ ($n=3$) can be thought of as a generalized version of the Fisher–KPP (Ginzburg–Landau) equation, modified through the presence of a spatio-temporally varying coefficient for the linear term. Generally, to obtain the significant 'on-off' type effects seen in biological signalling, the saturation effect must be weak, i.e. $\varepsilon\ll 1$. For ease of exposition, it is also

[1]For example, for a Turing bifurcation activated through a pitchfork with $n=3$, A typically represents the envelope amplitude for the patterned state, as predicted by the fastest growing mode at the onset of instability.

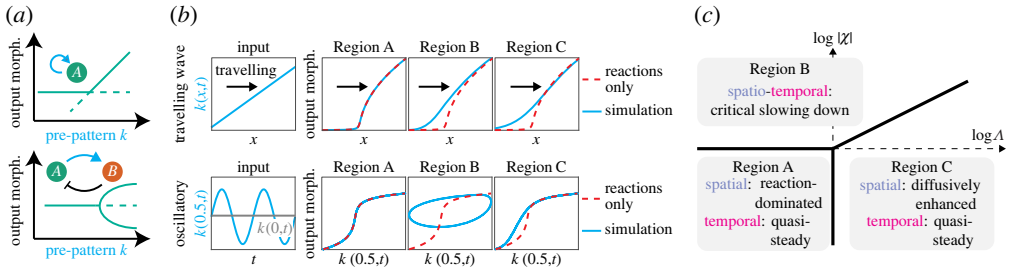

Figure 1. General asymptotic framework for classifying dynamics of pattern-forming systems. (*a*) Bifurcation diagrams and related minimal gene-regulatory network motifs for two classes of pattern-forming system. Top: autoinduction loops are associated with transcritical bifurcations. Bottom: activator-inhibitor systems are associated with pitchfork bifurcations. (*b*) Top: examples of predicted dynamics in three different regions of parameter space (see (*c*)) for a travelling gradient, the non-degenerate linearized form of more general spatio-temporal variations. Results were generated by solving equation (2.1) numerically, with $n = 3$ and $k(x, t)$ specified via $k(x, t) = x - t$. Results are similar for $n = 2$. The dashed line shows reaction-dominated results obtained by solving the steady form of equation (2.1) without diffusion. Bottom: examples of predicted dynamics for a spatio-temporal oscillation in $k(x, t)$ of the form $k(x, t) = -0.475 + x(1 + 0.25\sin(2\pi t))$, shown at a fixed x (left). Results were generated as in the top row, and plotted at $x = 0.5$ in a domain of size $x = 1$ (right; y axis log scale). In Region B, the system becomes locked in the patterned state despite large oscillations in $k(x, t)$. (*c*) General parameter space that classifies the system dynamics in each region for a general spatio-temporal variation. The boundary between Regions B and C occurs when $\Lambda^{2/3}/|\chi| = O(1)$ and $\Lambda, |\chi| \gg 1$.

convenient to impose $\omega \ll 1$ and $D \ll 1$, so that spatio-temporal variations in k appear to be locally quasi-steady in (2.1). We will show that, contrary to its appearance, the system (2.1) is not generally locally quasi-steady when crossing a bifurcation, and that this has significant implications for robustness over non-standard timescales. At this point, we make no further assumptions on the relative sizes of the small parameters ε, ω and D; we seek to understand all possible significant changes in system behaviour as the relative sizes of these parameters vary within the constraint of them being small.

Given the above, in the apparent locally quasi-steady system, $k < 0$ represents the unpatterned region (where $A \sim a/(-k) = O(1)$) and $k > 0$ the patterned region (where $A^{n-1} \sim k/\varepsilon \gg 1$), with $k = 0$ defining the position of the bifurcation in homogeneous conditions. These results correspond to the 'outer' regions away from the bifurcation (in the language of matched asymptotic expansions), where $A = O(1)$ corresponds to 'off' and $A^{n-1} = O(1/\varepsilon)$ corresponds to 'on'. However, we can immediately see that these locally quasi-steady outer solutions will not hold near $k = 0$, and this leads to the natural definition of the (moving) quasi-steady position of the bifurcation $x = s(t)$, defined through $k(s(t), t) = 0$. By examining the behaviour of the system near the bifurcation at $x = s(t)$, we will show that the system near the bifurcation is not generally locally quasi-steady, and we will see how and when this causes robustness to be generated in the system.

(a) Inner problem

To understand what happens near the moving bifurcation, we perform a local analysis. To do this, we transform into a moving interior layer around the point $x = s(t)$, which we recall is defined through $k(s(t), t) = 0$. The most straightforward type of motion to consider is a non-degenerate bifurcation moving monotonically, essentially a travelling-gradient-like motion. In this scenario, we have $\eta(t) := k_x(s(t), t) \neq 0$ and $\dot{s}(t) \neq 0$. We derive this scenario below, and analyse it in §3a. This analysis will elucidate the key types of possible behaviour near the moving bifurcation. The general ideas that arise from this monotonic analysis will be important later, when we consider the emergent robustness implications of our results for oscillating parameters. Since the bifurcation turns around in this latter scenario, its motion will not be monotonic and must be

treated separately. We therefore analyse this latter scenario separately, in §3b. Finally, for brevity, we focus largely on imperfect bifurcations in the main text below, but present the scalings and differences in analysis for perfect bifurcations in appendix A.

In scaling into the region near the moving bifurcation, we seek to derive a distinguished asymptotic limit and retain as much information as possible. To this end, we start by balancing the final three (reaction) terms in (2.1) to obtain the requisite scalings. This leads to the scaled independent and dependent variables $Z(x,t)=O(1)$ and $Y(Z,t)=O(1)$, respectively, defined through

$$x = s(t) + \frac{(a^{n-1}\varepsilon)^{1/n}}{\eta(t)} Z \quad \text{and} \quad A(x,t) = \left(\frac{a}{\varepsilon}\right)^{1/n} Y(Z,t), \tag{2.2}$$

emphasizing that $\varepsilon \ll 1$, so we are zooming into a region near $x = s(t)$. The balance between the final three (reaction) terms in (2.1) arises from the result

$$k(x,t) \sim (a^{n-1}\varepsilon)^{1/n} Z, \tag{2.3}$$

obtained by substituting (2.2) into $k(x,t)$, noting that $k(s(t),t)=0$, and Taylor expanding.

From the definition (2.2), derivatives are transformed as follows:

$$\frac{\partial}{\partial x} \mapsto \frac{\eta}{(a^{n-1}\varepsilon)^{1/n}} \frac{\partial}{\partial Z} \quad \text{and} \quad \frac{\partial}{\partial t} \mapsto \frac{\partial}{\partial t} + \left[\frac{\dot{\eta} Z}{\eta} - \frac{\eta \dot{s}}{(a^{n-1}\varepsilon)^{1/n}}\right] \frac{\partial}{\partial Z}. \tag{2.4}$$

Substituting (2.2)–(2.4) into (2.1), we obtain the transformed system

$$\frac{\omega}{(a^{n-1}\varepsilon)^{1/n}} \left(\frac{\partial Y}{\partial t} + \frac{\dot{\eta} Z}{\eta} \frac{\partial Y}{\partial Z} - \frac{\eta \dot{s}}{(a^{n-1}\varepsilon)^{1/n}} \frac{\partial Y}{\partial Z} \right) = \frac{\eta^2 D}{(a^{n-1}\varepsilon)^{3/n}} \frac{\partial^2 Y}{\partial Z^2} + 1 + ZY - Y^n. \tag{2.5}$$

Given that $\varepsilon \ll 1$ and $\eta, \dot{s} \neq 0$ for the non-degenerate moving bifurcation case we consider in this section, the first two terms in the brackets on the left-hand side are asymptotically sub-dominant to the third. Since we have made no further assumptions on the relative sizes of ε, ω and D beyond them being intrinsically small, we may consistently retain all remaining terms in order to capture as much information as possible, representing a distinguished asymptotic limit of the system. This procedure yields the leading-order system

$$0 = \Lambda(t) \frac{\partial^2 Y}{\partial Z^2} + \chi(t) \frac{\partial Y}{\partial Z} + 1 + ZY - Y^n, \tag{2.6a}$$

where

$$\Lambda(t) := \frac{\eta^2 D}{(a^{n-1}\varepsilon)^{3/n}} \quad \text{and} \quad \chi(t) := \frac{\eta \omega \dot{s}}{(a^{n-1}\varepsilon)^{2/n}}. \tag{2.6b}$$

Broadly, $\Lambda \in (0,\infty)$ quantifies the importance of diffusion and $\chi \in (-\infty,\infty)$ quantifies the importance of spatio-temporal changes in the parameters, both in comparison to base production. The sign of χ relates to whether the bifurcation is moving into the patterned or unpatterned region; the difference between these cases can be mathematically and biologically significant, as we will discuss later. By comparison with the classic normal forms for bifurcations in uniform conditions [33], the system (2.6*a*) corresponds to the (imperfect) normal form for a supercritical pitchfork bifurcation when $n=3$ and for a transcritical bifurcation when $n=2$, now in the presence of spatio-temporal variations.

Finally, we note that the appropriate far-field conditions can be obtained by matching into the outer (positive) quasi-steady solutions. In terms of the canonical equation (2.6), the consistent matching conditions are

$$Y \sim -\frac{1}{Z} \text{ as } Z \to -\infty \quad \text{and} \quad Y \sim Z^{1/(n-1)} \text{ as } Z \to +\infty. \tag{2.7}$$

3. Asymptotic analysis of canonical system

To fully characterize the possible behaviours of the transition across the bifurcation, we seek to understand the possible behaviours of Y in terms of Λ and χ. One way to do this is to examine the

distinguished asymptotic limits of the ODE system (2.6) and (2.7). This approach has the benefit of enabling us to derive analytic leading-order solutions, which will allow us to explicitly quantify the effect of crossing the bifurcation.

To provide some context to signpost the technical analysis we present shortly, we now briefly summarize the asymptotic structure of the solution space we explore below. As outlined in figure 1*c*, there are three sublimits in the system (in terms of asymptotic values of Λ and χ) labelled Regions A–C, and each separated by distinguished limits of the system. Each sublimit corresponds to the overall domination of one of the three physical drivers within the inner transition region: positive feedback, diffusion and spatio-temporal variations in the parameters. Given that we are interested in understanding how the solution varies away from the quasi-steady solution dominated by positive feedback, it is helpful to define the point $Z = Z^*$ at which $Y(Z^*) = 1$. We refer to this as the dynamical position of the bifurcation. We will show below that $Z^* = 0$ for the straightforward quasi-steady solution, but that $Z^* \neq 0$ when diffusive and spatio-temporal variations are important in the system.

For pitchfork bifurcations ($n = 3$), which can arise from e.g. activator-inhibitor Turing systems, a key question is whether the patterned regions remain robust under spatio-temporal variations involving incursions from the encroaching unpatterned state (on-to-off). This corresponds to the bifurcation moving from the unpatterned to the patterned state ($\chi > 0$). For transcritical bifurcations ($n = 2$), which can arise from e.g. self-activator systems, a key question is whether unpatterned regions remain robust under spatio-temporal variations involving incursions from the patterned state (off-to-on). This corresponds to the bifurcation moving from the patterned to the unpatterned state ($\chi < 0$). While the specific details of the analysis will depend on whether the bifurcation is moving towards the patterned or the unpatterned region, the appropriate scalings for the distinguished limits and sublimits outlined in figure 1*c* hold in either case. In an effort to balance breadth and brevity of analysis, we therefore limit ourselves here to considering the two physically relevant cases mentioned above. We present the pitchfork case ($n = 3$) with $\chi > 0$ in the main text below, and the transcritical case ($n = 2$) with $\chi < 0$ in appendix B.

As justified at the start of §2a, in the following, we first analyse the three regimes that arise from travelling-wave-like variation of the system parameters (i.e. monotonic, unidirectional motion of the bifurcation), and then analyse the scenario with spatio-temporally oscillating parameters (i.e. where the bifurcation turns around). Together, these encompass a significant class of behaviours the moving bifurcation can exhibit.

(a) Travelling-wave-like parameter variations for on-to-off pitchfork bifurcations

In this subsection, we consider pitchfork bifurcations ($n = 3$), where the bifurcation moves unidirectionally from the unpatterned to patterned state ($\chi > 0$). This corresponds to 'on-to-off' patterning. The pitchfork analysis involves the governing equation (2.6), taking $n = 3$, with far-field conditions (2.7).

We re-emphasize that in this section, we are specifically interested in asymptotic solutions for $\chi > 0$, and the analytic results we obtain for Y and Z^* are specific to this case. However, the asymptotic scalings we derive and summarize later in §3a(iv) will be the same for $\chi < 0$. We proceed by analysing each parameter region in increasing order of complexity.

(i) Positive feedback dominates: Region A

The simplest region is Region A, where $\Lambda, \chi \ll 1$. Hence, positive feedback dominates here, and the solution remains quasi-steady through the bifurcation. In this case, the ODE (2.6) becomes quasi-steady, and at leading-order Y is defined implicitly through the cubic equation

$$1 + ZY - Y^3 = 0. \tag{3.1}$$

We note that, if required, an explicit solution to (3.1) can be obtained straightforwardly by invoking the cubic formula. In this quasi-steady limit, $Y(0) = 1$, and therefore $Z^* = 0$. This is also

the regime for a stationary bifurcation when diffusive effects are not significant. Hence, in Region A, the bifurcation takes its equilibrium position as we would expect from a quasi-steady analysis, and the patterning is spatially local and quasi-steady.

The solutions in the remainder of parameter space will be significantly different to Region A. In particular, there will be sharp transitions between the unpatterned and patterned parts of the transition region, and in general, these transitions will not occur around $Z = 0$.

(ii) Spatio-temporal variations dominate: Region B

Region B occurs when $\chi \gg 1$ and $\Lambda/\chi^{3/2} \ll 1$. In this region, spatio-temporal changes in the parameters dominate and delaying effects become important, with implications for pattern robustness. Importantly, in this region, there are sharp transitions between the unpatterned and patterned parts of the transition region, separated by $Z = Z_c$ (which we shall see is different but related to Z^*).

To summarize the asymptotic structure of the solution before going into the specific mathematical analysis—in Region B, the interesting behaviour occurs over the lengthscale $Z = O(\sqrt{\chi})$, so we scale into a new independent variable $\sigma = Z/\sqrt{\chi}$. The asymptotic solution is then split into two asymptotic regions separated by the point $\sigma = \sigma_c := Z_c/\sqrt{\chi}$. The determination of σ_c and Z^* are key goals of our analysis. The unpatterned region corresponds to $\sigma < \sigma_c$ and the patterned region corresponds to $\sigma > \sigma_c$. The solution is smaller in the unpatterned region, with the scaling $Y = Y_L/\sqrt{\chi}$, and larger in the patterned region, with the scaling $Y = \chi^{1/4} Y_R$.

Here, information travels in the same direction as the pattern transition, i.e. from the patterned state to the unpatterned state (on-to-off). As such, our analysis starts in the patterned state, where $\sigma > \sigma_c$. Using the scalings noted above, the leading-order scaled version of the ODE system (2.6) and (2.7) in the patterned state is

$$0 = \frac{\partial Y_R}{\partial \sigma} + \sigma Y_R - Y_R^3, \quad Y_R \sim \sqrt{\sigma} \text{ as } \sigma \to \infty. \tag{3.2}$$

We can solve (3.2) explicitly by multiplying through by Y_R, and introducing the new dependent variable $W(\sigma)$ such that $Y_R^2 = -W'/(2W)$. The ODE (3.2) then transforms to

$$0 = W'' + 2\sigma W', \quad \frac{W'}{W} \sim -2\sigma \text{ as } \sigma \to \infty. \tag{3.3}$$

The two linearly independent solutions to the ODE in (3.3) are $\operatorname{erfc}(\sigma)$ and 1, where erfc is the complementary error function. Applying the far-field condition in (3.3) removes the possibility of any contribution from the constant solution, leading to the solution $W = \alpha \operatorname{erfc}(\sigma)$ for constant α, and hence

$$Y_R = \frac{\mathrm{e}^{-\sigma^2/2}}{\pi^{1/4}\sqrt{\operatorname{erfc}\sigma}}. \tag{3.4}$$

For later matching purposes, we note the following far-field result from (3.4):

$$Y_R \sim \frac{\mathrm{e}^{-\sigma^2/2}}{(4\pi)^{1/4}} \quad \text{as } \sigma \to -\infty. \tag{3.5}$$

Given the relative scalings of Y in the patterned and unpatterned regions, we can determine σ_c by calculating when $Y_R = O(\chi^{-3/4})$. From the far-field result (3.5), this occurs when $\sigma = \sigma_c \sim -\sqrt{\log \chi^{3/2}}$.

For completeness, we now also provide the solution in the unpatterned state, where $\sigma < \sigma_c$. Using the scalings noted above for the unpatterned state, the leading-order scaled version of the ODE system (2.6), (2.7) in the unpatterned state is

$$0 = \frac{\partial Y_L}{\partial \sigma} + 1 + \sigma Y_L, \tag{3.6}$$

with an additional condition that will arise from matching with the solution (3.4) in the patterned state. Using the integrating factor method, the ODE (3.6) is solved by

$$Y_L = \beta\, \mathrm{e}^{-\sigma^2/2} + F\left(\frac{\sigma}{\sqrt{2}}\right), \tag{3.7}$$

where $F(x)$ is Dawson's integral [39, eqn. 7.2.5], defined as

$$F(x) := \mathrm{e}^{-x^2} \int_0^x \mathrm{e}^{s^2}\, \mathrm{d}s, \tag{3.8}$$

and β is a constant to be determined through matching with (3.4). Since Dawson's integral (3.8) is bounded along the entire real line, the matching procedure does not involve this term and is therefore fairly straightforward. Using the far-field limit of the patterned solution (3.5), and recalling that the intrinsic solution scalings are $Y = Y_L/\sqrt{\chi}$ and $Y = \chi^{1/4} Y_R$, we find that

$$\beta = \frac{\chi^{3/4}}{(4\pi)^{1/4}}, \tag{3.9}$$

completing the solution (3.7).

Finally, we calculate the dynamic position of the bifurcation $Z^* = \sqrt{\chi}\sigma^*$, defined through $Y(Z^*) = 1$ and hence through $Y_R(\sigma^*) = \chi^{-1/4}$. From (3.5), this occurs for $\sigma^* \sim -\sqrt{\log \chi^{1/2}}$. Scaling back into Z^*, we obtain the following asymptotic result for the dynamic position of the bifurcation:

$$Z^* \sim -\sqrt{\frac{\chi \log \chi}{2}} \quad \text{for } \chi \gg 1 \text{ and } \Lambda/\chi^{3/2} \ll 1 \text{ (Region B)}. \tag{3.10}$$

(iii) Diffusion dominates: Region C

Region C occurs when $\Lambda \gg 1$ and $\Lambda/\chi^{3/2} \gg 1$. In this region, diffusive effects dominate. This is also the regime for a stationary bifurcation when diffusive effects are significant. In a similar manner as for Region B, there are sharp transitions between the unpatterned and patterned parts of the transition region here, separated by $Z = Z_c$ (which again is different but related to Z^*).

To summarize the asymptotic structure of the solution—in Region C, the interesting behaviour occurs over the lengthscale $Z = O(\Lambda^{1/3})$, so we scale into a new independent variable $\zeta = Z/\Lambda^{1/3} = O(1)$. The solution is again split into two asymptotic regions, matched using an intermediate transition region. This time, the two main asymptotic regions are separated by the point $\zeta = \zeta_c := Z_c/\Lambda^{1/3}$. The determination of ζ_c and Z^* are key goals of our analysis. The unpatterned region corresponds to $\zeta < \zeta_c$ and the patterned region corresponds to $\zeta > \zeta_c$. The solution is smaller in the unpatterned region, with the scaling $Y = W_L/\Lambda^{1/3}$, and larger in the patterned region, with the scaling $Y = \Lambda^{1/6} W_R$.

Using the scalings noted above, the leading-order scaled version of the system (2.6) and (2.7) in the patterned state ($\zeta > \zeta_c$) is

$$\frac{\partial^2 W_R}{\partial \zeta^2} + \zeta W_R - W_R^3 = 0, \quad W_R \sim \sqrt{\zeta} \text{ as } \zeta \to \infty. \tag{3.11}$$

Similarly, the leading-order scaled version of the system (2.6), (2.7) in the unpatterned state ($\zeta < \zeta_c$) is

$$\frac{\partial^2 W_L}{\partial \zeta^2} + \zeta W_L + 1 = 0, \quad W_L \sim -\frac{1}{\zeta} \text{ as } \zeta \to -\infty. \tag{3.12}$$

Since the nonlinear ODE in (3.11) is second order, it is more difficult to obtain an analytic solution within the patterned region than it was for Region B. However, we can solve (3.12)

straightforwardly using the variation of parameters method to obtain

$$W_L = c_L \,\mathrm{Ai}(-\zeta) + P(\zeta), \tag{3.13}$$

where the constant c_L can be obtained via matching with the solution in the patterned region, and where the function $P(\zeta)$ is defined as

$$P(\zeta) = \pi \left[\mathrm{Bi}(-\zeta) \int_{-\infty}^{\zeta} \mathrm{Ai}(-s)\,\mathrm{d}s - \mathrm{Ai}(-\zeta) \int_{0}^{\zeta} \mathrm{Bi}(-s)\,\mathrm{d}s \right], \tag{3.14}$$

and is related to the Scorer functions [39, Sec. 9.12].

Given the relative scalings of Y in each asymptotic region, we can determine the position $\zeta = \zeta_c$ by calculating when $W_R = O(\Lambda^{-1/2})$. Similarly, the dynamic position of the bifurcation $Z^* = \Lambda^{1/3}\zeta^*$ can be inferred through the relationship $Y(Z^*) = 1$, and hence $W_R(\zeta^*) = \Lambda^{-1/6}$. Hence, we require knowledge of the decaying behaviour of the nonlinear ODE (3.11) as we move towards the unpatterned far-field $\zeta \to -\infty$. Linearizing (3.11) around the far-field trivial solution and imposing decay results in the behaviour

$$W_R \sim c_R \,\mathrm{Ai}(-\zeta), \quad \text{as } \zeta \to -\infty, \tag{3.15}$$

where c_R is an $O(1)$ constant, which is straightforward to determine numerically if required. (Matching with the unpatterned region gives the relationship $c_L = \Lambda^{1/2} c_R$.)

Using the far-field behaviour of the Airy function, determining when $W_R = O(\Lambda^{-1/2})$ yields $\zeta_c \sim -(\log \Lambda^{3/4})^{2/3}$ and determining when $W_R(\zeta^*) = \Lambda^{-1/6}$ yields $\zeta^* \sim -(\log \Lambda^{1/4})^{2/3}$, resulting in the following asymptotic result for the dynamic position of the bifurcation:

$$Z^* \sim -\left(\frac{\Lambda \log^2 \Lambda}{16}\right)^{1/3} \quad \text{for } \Lambda \gg 1 \text{ and } \frac{\Lambda^{3/2}}{\chi} \gg 1 \text{ (Region C).} \tag{3.16}$$

(iv) Summary

Our results suggest that the emergent dynamics of pattern-forming systems are determined in time and space by the regime in which the parameters lie (figure 1*b*,*c*). Furthermore, our results *quantify* how the location of a dynamic bifurcation is determined in each regime—either purely by a balance between the reaction terms for Region A, or otherwise for Regions B and C (figure 1*b*,*c*). In Regions B and C, diffusion and temporal variations in the parameters promote shifts in the location of the bifurcation which we quantify using an asymptotic analysis. While we give the specific (quantitative) asymptotic results in each section, the scalings for both pitchfork and transcritical bifurcations are similar and can be summarized as follows:

Region A. Reaction-dominated and quasi-steady patterning. In this case, $\Lambda \ll 1$ and $|\chi| \ll 1$, and the reaction terms (iii)–(v) dominate in (2.6). This is also the regime for a stationary bifurcation when diffusive effects are not significant. The dynamical position of the bifurcation corresponds to its quasi-steady position, i.e. $Z^* = 0$ (figure 1*b*,*c*).

Region B. Critical slowing down. In this case $|\chi| \gg 1$ and $\Lambda^{2/3}/|\chi| \ll 1$, and terms (ii)–(v) dominate in (2.6)—saturation, i.e. term (v), can be ignored in the unpatterned part of the domain, and base production, i.e. term (iii), can be ignored in the patterned part. The dynamical position of the bifurcation lags behind its quasi-steady position, and scales as $|Z^*| = O(\sqrt{|\chi| \log |\chi|})$ (figure 1*b*,*c*).

Region C. Diffusively enhanced, quasi-steady patterning. In this case $\Lambda \gg 1$ and $\Lambda^{2/3}/|\chi| \gg 1$, and terms (i), (iii)–(v) dominate in (2.6)—saturation can be ignored in the unpatterned part of the domain, and base production can be ignored in the patterned part. This is also the regime for a stationary bifurcation when diffusive effects are significant. The dynamical position of the bifurcation is shifted via diffusion towards the unpatterned part of the domain, and scales as $|Z^*| = O((\Lambda \log^2 \Lambda)^{1/3})$ (figure 1*b*,*c*).

(b) Spatio-temporal parameter oscillations for pitchfork bifurcations

In the previous subsection, we calculate the dynamic location of the bifurcation and hence the effective delay caused by travelling-wave-like spatio-temporal variations (i.e. *monotonically* moving bifurcations), identifying and analysing three distinct parameter regions in space that demonstrate different types of behaviour. However, there are also important questions regarding robustness in biological systems involving oscillatory spatio-temporal variations, i.e. *non-monotonically* moving bifurcations. As a key example of this—consider the situation where spatio-temporal variations in system coefficients would cause the system (at a fixed position in space) to move back and forth between the patterned and unpatterned regions predicted by a quasi-steady analysis (i.e. a local balance between reaction terms). How does the persistence or decay of the patterning depend on the spatio-temporal variation in the system? And can the delaying effects quantified in the previous section cause an effective robustness of the system to spatio-temporal variations over non-standard intermediate timescales, as seen in §3a? Quantitative answers to such questions are not covered by the analysis in §3a, which was restricted to monotonic bifurcation movement.

To determine whether non-monotonic moving bifurcations can have a significant effect on pattern persistence, we perform a preliminary numerical investigation of the effect of oscillatory variations in the system (2.1) (figure 1*b*). We find that there is an effective hysteresis associated with oscillating over the bifurcation, and so each system may indeed become stuck in the unpatterned or patterned state (figure 1*b*) for parameters oscillating quickly enough, even at large amplitude oscillations. This suggests that the bifurcations in each system can act as low-pass filters on parameter variations.

To understand why this happens and to quantify the phenomenon, we now investigate the system around a *fixed* position in space, in cases where the moving bifurcation turns around. Again, with the aim of balancing breadth and brevity, we consider the biologically relevant cases of patterned-unpatterned-patterned for pitchfork bifurcations ($n=3$) in the main text, and unpatterned-patterned-unpatterned for transcritical bifurcations ($n=2$) in appendix B(b). Moreover, since we are specifically concerned with robustness to spatio-temporal variations, we restrict our analysis here to the 'critical slowing down' regime. This is the equivalent of Region B from the previous subsection, in which dynamics are slowed by passage through the bifurcation [34]. Specifically, this means we consider the scenario where diffusive effects are less important. However, we will retain the generality of the spatio-temporal variations by preserving their full nature and resisting the temptation to expand them locally in space and time.

(i) Deriving inner equation

Here, we consider (2.1) with $n=3$, which produces a pitchfork bifurcation. Hence, we start with the system

$$\omega\frac{\partial A}{\partial t}=D\frac{\partial^2 A}{\partial x^2}+a+k(x,t)A-\varepsilon A^3. \tag{3.17}$$

We are specifically interested in spatio-temporal oscillations of $k(x,t)$ (i.e. cases where the bifurcation can turn around) and in understanding the intrinsic robustness of patterning due to this non-monotonically moving bifurcation. As such, we zoom into a region near the generic fixed point $x=x^*$, around the time $t=t^*$ at which the bifurcation reaches the fixed point, defined through $k(x^*,t^*)=0$. We consider the scenario where the point $x=x^*$ transitions from patterned-unpatterned-patterned under a quasi-steady analysis (i.e. a local balance between reaction terms). Mathematically, this corresponds to $k(x^*,t)$ transitioning from positive-negative-positive. When $k<0$, there is a drive to de-pattern. Since we are specifically interested in understanding when the system demonstrates intrinsic robustness, we are interested in understanding when the system overcomes this forcing to de-pattern and patterning persists. Therefore, we investigate when the critical slowing down effect of Region B presented in §3a can overcome this forcing before k becomes positive again and the system returns to the locally patterned state. That is,

quantifying when the system is robust to temporary incursions into regimes that would appear to be unpatterned from a quasi-steady analysis.

Since we are focusing on the critical slowing down scenario, diffusive effects can be neglected. As such, we can effectively consider $D = 0$ in (3.17) and in what follows. However, we retain D for the time being in order to understand when we can formally neglect it. As before, we treat ω and ε as small.

We are specifically interested in understanding when forcing transitions from patterned-unpatterned-patterned resist de-patterning and remain patterned, so the key terms in (3.17) are the left-hand side and the final two terms on the right-hand side. While we will formalize this intuitive dominant balance for the specific scenarios in which we are interested below, it is helpful to note that for this dominant balance all relevant asymptotic scalings will reduce (3.17) to an equation of the form

$$\frac{\partial Y}{\partial T} = \bar{k}(X,T)Y - Y^3, \quad Y(X,T) \sim \sqrt{\bar{k}(X,T)} \text{ as } T \to -\infty, \tag{3.18}$$

at leading-order, for appropriately defined independent variables X, T, dependent variable $Y(X,T)$, and function $\bar{k}(X,T)$, noting that $\bar{k} > 0$ as $T \to -\infty$. It is straightforward to solve (3.18) by introducing $W(X,T)$, defined through the transformation $Y^2 = (\partial W/\partial T)/(2W)$, to turn (3.18) into

$$\frac{\partial^2 W}{\partial T^2} - 2\bar{k}(X,T)\frac{\partial W}{\partial T} = 0, \quad \frac{W_T}{2W} \sim \bar{k}(X,T) \text{ as } T \to -\infty, \tag{3.19}$$

which can be solved in terms of $\bar{k}(X,T)$, and transformed back into a solution for Y as follows:

$$Y = \frac{\exp(\bar{K}(X,T))}{\left(2\int_{-\infty}^{T} \exp(2\bar{K}(X,s))\,\mathrm{d}s\right)^{1/2}} \quad \text{where } \bar{K}(X,T) := \int_0^T \bar{k}(X,s)\,\mathrm{d}s. \tag{3.20}$$

(ii) Fixed away from the turning point

We first consider the case where $k_t(x^*,t^*) \neq 0$ i.e. the position at which the bifurcation turns around is away from the fixed point $x = x^*$. In this case, the appropriate inner equation scalings into the initially patterned region are

$$x = x^* + \sqrt{\omega}X, \quad t = t^* + \sqrt{\omega}T \quad \text{and} \quad A = \frac{\omega^{1/4}}{\varepsilon^{1/2}}Y. \tag{3.21}$$

These scalings turn (3.17) into

$$\frac{\partial Y}{\partial T} = \frac{\widehat{\Lambda}}{\widehat{\chi}^{3/2}}\frac{\partial^2 Y}{\partial X^2} + \frac{1}{\widehat{\chi}^{3/4}} + \bar{k}(X,T)Y - Y^3, \tag{3.22}$$

where we introduce the parameter groupings

$$\widehat{\Lambda} := \frac{D}{a^2\varepsilon} \quad \text{and} \quad \widehat{\chi} = \frac{\omega}{(a^2\varepsilon)^{2/3}}, \tag{3.23}$$

keeping similar notation as in (2.6*b*), and the function

$$\bar{k}(X,T) := \frac{k(x^* + \sqrt{\omega}X, t^* + \sqrt{\omega}T)}{\sqrt{\omega}}. \tag{3.24}$$

We note that $\bar{k} = O(1)$ since $k(x^*,t^*) = 0$. Moreover, while it is possible to replace the right-hand side of (3.24) with its linearization for many differentiable functions k, we keep it in its general form since we are specifically interested in oscillations in T. That is, we are specifically interested in $\bar{k}$ with turning points in T, and these will generally not be well-approximated by their linearizations.

The formal neglect of the diffusive and base production terms in (3.22) correspond to the limits $\widehat{\chi} = \omega/(a^2\varepsilon)^{2/3} \gg 1$ and $\widehat{\Lambda}/\widehat{\chi}^{3/2} = D/\omega^{3/2} \ll 1$, directly analogous to the limits that take us into Region B in the previous section. Moreover, this limit reduces (3.22) to the system (3.18), which

is solved by (3.20). We can calculate when Y reaches a critical minimal value (specified by the particular problem being considered) via simple one-dimensional root finding of the asymptotic solution (3.20) (see electronic supplementary material, figure S1). While there will be additional asymptotic regions (analogous to their Region B versions) as Y becomes smaller for both imperfect and perfect pitchforks, we expect practical de-patterning to occur before these regions are reached so do not consider them further.

(iii) Fixed at the turning point

We now consider the case where $k_t(x^*, t^*) = 0$ and $k_{tt}(x^*, t^*) > 0$ i.e. the bifurcation turns around at the fixed point $x = x^*$. In this case, the appropriate inner equation scalings into the initially patterned region are

$$x = x^* + \omega^{2/3} X, \quad t = t^* + \omega^{1/3} T \quad \text{and} \quad A = \frac{\omega^{1/3}}{\varepsilon^{1/2}} Y. \tag{3.25}$$

These scalings turn (3.17) into

$$\frac{\partial Y}{\partial T} = \frac{\widehat{\Lambda}}{\tilde{\chi}^{3/2}} \frac{\partial^2 Y}{\partial X^2} + \frac{1}{\tilde{\chi}^{3/4}} + \tilde{k}(X, T) Y - Y^3, \tag{3.26}$$

where $\widehat{\Lambda}$ is defined in (3.23), and we introduce the parameter grouping

$$\tilde{\chi} = \frac{\omega^{4/3}}{(a^2 \varepsilon)^{2/3}} = \omega^{1/3} \widehat{\chi}, \tag{3.27}$$

where $\widehat{\chi}$ is defined in (3.23), as well as the function

$$\tilde{k}(X, T) := \frac{k(x^* + \omega^{2/3} X, t^* + \omega^{1/3} T)}{\omega^{2/3}}. \tag{3.28}$$

We note that $\tilde{k} = O(1)$ since $k(x^*, t^*) = k_t(x^*, t^*) = 0$. Moreover, while it is possible to replace (3.28) with $\tilde{k}(X, T) \sim k_x X + k_{tt} T^2/2$ (with partial derivatives of k evaluated at (x^*, t^*)) for many differentiable functions k, we keep it in the form (3.28) for generality.

The formal neglect of the diffusive and base production terms in (3.26) correspond to the limits $\tilde{\chi} = \omega^{4/3}/(a^2\varepsilon)^{2/3} \gg 1$ and $\widehat{\Lambda}/\tilde{\chi}^{3/2} = D/\omega^2 \ll 1$. We note that both these constraints represent slightly stricter requirements on ω than their equivalents in the previous subsection, where we investigated a fixed position *away* from the turning point. Broadly, these constraints both require ω to be slightly larger than in the previous subsection for equivalent remaining parameters; this is because the constraints generally require $\tilde{\chi}$ (and hence ω) to be large enough, and $\tilde{\chi}$ is a factor of $\omega^{1/3}$ smaller than $\widehat{\chi}$, so needs to compensate. If these constraints are satisfied, this limit again reduces (3.26) to the system (3.18), which is solved by (3.20).

4. Biological example: Turing patterns during development

We apply our analytic results and perform simulations in the context of two paradigmatic biological pattern-forming systems with variations in pre-pattern morphogens. In each case, the morphogen variations affect parameters in the system gene-regulatory network [8]. In the main text here, we consider a model for digit formation via activator-inhibitor Turing patterns [18], which is associated with a pitchfork bifurcation. In the electronic supplementary material, we consider a model for bacterial quorum sensing (QS) in *Vibrio fischeri*, which causes bioluminescence in the Hawaiian bobtail squid [40]. The bacterial QS system is associated with a transcritical bifurcation.

(a) Mathematical model

We consider digit formation in the embryo, which has been modelled as a Turing system [18]. This system is associated with a pitchfork bifurcation. The kinetic parameters of the system are

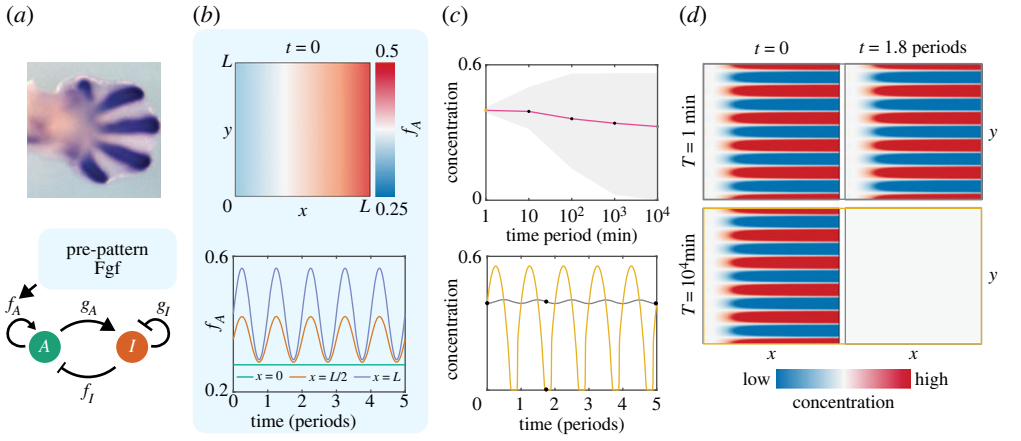

Figure 2. Effect of spatio-temporal morphogen variations on Turing patterns. (*a*) We model Turing patterns during digit formation (top; reproduced from [18] with permission). The system's pattern can be represented as an activator-inhibitor system, with the self-activation parameter f_A modulated by a morphogen called Fgf (bottom). (*b*) The parameter f_A (min^{-1}) at $t = 0$ (top) and throughout the spatio-temporal oscillations (4.3) (bottom; electronic supplementary material, movie S1). (*c*) Top: effect of time period $\tilde{\tau}$ of spatio-temporal oscillations in Fgf on the mean concentration of the activator morphogen (line), and the range of concentration (grey area) during the oscillations. Bottom: oscillations in the activator morphogen concentration for fast ($\tilde{\tau} = 1$ min) and slow ($\tilde{\tau} = 10^4$ min) oscillations in Fgf (electronic supplementary material, movie S1). (*d*) For oscillations that are filtered out, patterning remains the same (top). For oscillations that are not filtered out, patterning completely disappears (bottom). Images correspond to the black dots in panel c. Concentrations in the figure are non-dimensional and represent deviation from a base state at $x = 0$ [20].

controlled by a spatio-temporally varying morphogen called fibroblast growth factor (Fgf) [18], which affects the self-activation of the activator (figure 2*a*). For a minimalistic representation, and following a model in [18], we ignore the effects of other morphogens that are thought to affect the system. The assumption of a hierarchical system in which a pre-pattern morphogen controls the dynamics of downstream morphogens is also in line with experimental results in other biological systems [25]. We expect our results to extend to more complicated systems that account for more morphogens and more complicated gene-regulatory networks [10,20].

The digit formation example we consider in this section is described by the system

$$\frac{\partial \tilde{A}}{\partial \tilde{t}} = \tilde{\nabla} \cdot (\tilde{D}_A \tilde{\nabla} \tilde{A}) + \tilde{f}_A \left(\frac{\tilde{x}}{\tilde{L}}, \frac{\tilde{t}}{\tilde{\tau}} \right) \tilde{A} - \tilde{f}_I \tilde{I} - \tilde{f}_c \tilde{A}^3 \tag{4.1a}$$

$$\frac{\partial \tilde{I}}{\partial \tilde{t}} = \tilde{\nabla} \cdot (\tilde{D}_I \tilde{\nabla} \tilde{I}) + \tilde{g}_A \tilde{A} - \tilde{g}_I \tilde{I}, \tag{4.1b}$$

where the tildes denote dimensional quantities. We impose no-flux boundary conditions on the exterior of the domain

$$\boldsymbol{n} \cdot (\tilde{D}_A \tilde{\nabla} \tilde{A}) = 0 \quad \text{and} \quad \boldsymbol{n} \cdot (\tilde{D}_I \tilde{\nabla} \tilde{I}) = 0. \tag{4.1c}$$

Here, $\tilde{A}$ and $\tilde{I}$ are the concentrations of the activator and inhibitor, respectively, $\tilde{D}_A$ and $\tilde{D}_I$ are diffusion coefficients, and $\tilde{f}_A, \tilde{f}_I, \tilde{g}_A, \tilde{g}_I$ and $\tilde{f}_c$ are kinetic parameters (figure 2*a*). To simulate spatio-temporal variations in Fgf [18], we let $\tilde{f}_A(\tilde{x}/\tilde{L}, \tilde{t}/\tilde{\tau})$ vary in space and time:

$$\tilde{f}_A \left(\frac{\tilde{x}}{\tilde{L}}, \frac{\tilde{t}}{\tilde{\tau}} \right) = \tilde{f}_A^b + \tilde{k}_A f \left(\frac{\tilde{x}}{\tilde{L}}, \frac{\tilde{t}}{\tilde{\tau}} \right), \tag{4.2}$$

where $\tilde{f}_A^b$ is the base self-activation of the activator, $\tilde{k}_A$ is a typical increase in the self-activation, and $f(\tilde{x}/\tilde{L}, \tilde{t}/\tilde{\tau})$ is a non-dimensional concentration of Fgf. Here, $\tilde{L}$ and $\tilde{\tau}$ are typical lengthscales

and timescales of the variation. For the numerical simulations we present in figure 2, we consider the system (4.1) in two spatial dimensions, but we restrict our analysis of the system to one spatial dimension.

We will generally use either

$$f\left(\frac{\tilde{x}}{\tilde{L}},\frac{\tilde{t}}{\tilde{\tau}}\right)=\left(1+K\sin\left(\frac{2\pi\tilde{t}}{\tilde{\tau}}\right)\right)\frac{\tilde{x}}{\tilde{L}} \tag{4.3}$$

$$\text{or}\quad f\left(\frac{\tilde{x}}{\tilde{L}},\frac{\tilde{t}}{\tilde{\tau}}\right)=\frac{\tilde{x}}{\tilde{L}}-\frac{\tilde{t}}{\tilde{\tau}}, \tag{4.4}$$

and we note that $f=\tilde{x}/\tilde{L}$ reduces to a system similar to the steady system studied in [18]. As an initial condition, we use the steady-state patterned solution for $K=0$, with stripes oriented parallel to $\tilde{x}$, to test the effect of oscillations in Fgf on the patterns investigated in [18]. For simplicity, we use the same parameters as [18] for all kinetic parameters (electronic supplementary material, table S1). For the oscillation case (4.3), we set $K=0.9$ to represent an oscillation in chemical concentration of around 90% over a timescale $\tilde{\tau}$; the aim is to find the critical $\tilde{\tau}$ for which the oscillation is observed in the pattern-forming reactants.

(b) Non-dimensional problem

We non-dimensionalize the one-dimensional version of (4.1) using

$$\tilde{t}=\tilde{\tau}t,\quad \tilde{x}=\tilde{L}x,\quad \tilde{A}=\frac{\tilde{g}_I^{1/2}\varepsilon^{1/2}}{\tilde{f}_c^{1/2}}A\quad\text{and}\quad \tilde{I}=\frac{\tilde{g}_A\varepsilon^{1/2}}{\tilde{g}_I^{1/2}\tilde{f}_c^{1/2}}I, \tag{4.5}$$

where the concentration scalings have been chosen to scale straightforwardly into the forthcoming weakly nonlinear analysis. The scalings (4.5) transform (4.1) into the system

$$\omega\frac{\partial A}{\partial t}=\mathrm{d}\varepsilon^3\frac{\partial^2 A}{\partial x^2}+\lambda(1+rf(x,t))A-\gamma I-\varepsilon A^3 \tag{4.6a}$$

$$\omega\frac{\partial I}{\partial t}=\varepsilon^3\frac{\partial^2 I}{\partial x^2}+A-I, \tag{4.6b}$$

with

$$\frac{\partial A}{\partial x}=0\quad\text{and}\quad\frac{\partial I}{\partial x}=0,\quad\text{on } x=0,1, \tag{4.6c}$$

where we have introduced the dimensionless parameters

$$\varepsilon=\left(\frac{\tilde{D}_I}{\tilde{g}_I\tilde{L}^2}\right)^{1/3},\quad d=\frac{\tilde{D}_A}{\tilde{D}_I},\quad \omega=\frac{1}{\tilde{g}_I\tilde{\tau}},\quad \lambda=\frac{\tilde{f}_A^b}{\tilde{g}_I},\quad r=\frac{\tilde{k}_A}{\tilde{f}_A^b}\quad\text{and}\quad \gamma=\frac{\tilde{f}_I\tilde{g}_A}{\tilde{g}_I^2}. \tag{4.7}$$

We will proceed by reducing this system to its inner normal form, via a systematic asymptotic analysis in which we formally exploit the small parameters $\varepsilon,\omega\ll 1$.

(c) Reduction to normal form

(i) Travelling-wave-like parameter variations

The relevant inner scalings for this problem involve two spatial lengthscales. These consist of a short scale X that characterizes the small wavelength of patterns, and an intermediate scale σ that characterizes the (more) slowly varying amplitude of the patterns. Mathematically, these are defined as

$$X=\frac{x}{\varepsilon^{3/2}}\quad\text{and}\quad\sigma=\frac{x-s(t)}{\varepsilon}, \tag{4.8}$$

where the $O(\varepsilon^{3/2})$ scaling for X is determined by balancing the diffusive terms with the linear reaction terms, and the $O(\varepsilon)$ scaling for σ is determined by balancing the linear reaction terms

with the nonlinear saturation terms. The scalings (4.8) transform the governing equations (4.6) into the system

$$\omega\frac{\partial A}{\partial t}-\frac{\omega\dot{s}}{\varepsilon}\frac{\partial A}{\partial \sigma}=d(A_{XX}+2\varepsilon^{1/2}A_{X\sigma}+\varepsilon A_{\sigma\sigma})+\lambda(1+rf(s(t)+\varepsilon\sigma,t))A-\gamma I-\varepsilon A^3 \tag{4.9a}$$

$$\omega\frac{\partial I}{\partial t}-\frac{\omega\dot{s}}{\varepsilon}\frac{\partial I}{\partial \sigma}=(I_{XX}+2\varepsilon^{1/2}I_{X\sigma}+\varepsilon I_{\sigma\sigma})+A-I. \tag{4.9b}$$

We proceed by considering an asymptotic expansion in powers of $\varepsilon^{1/2}$

$$\boldsymbol{A}\sim\boldsymbol{A}_0+\varepsilon^{1/2}\boldsymbol{A}_1+\varepsilon\boldsymbol{A}_2=\begin{pmatrix}A_0(X,\sigma,t)\\ I_0(X,\sigma,t)\end{pmatrix}+\varepsilon^{1/2}\begin{pmatrix}A_1(X,\sigma,t)\\ I_1(X,\sigma,t)\end{pmatrix}+\varepsilon\begin{pmatrix}A_2(X,\sigma,t)\\ I_2(X,\sigma,t)\end{pmatrix}, \tag{4.10}$$

where the leading-order solution can be obtained through a straightforward linear analysis of the system. The parameter $\omega\ll 1$; it is convenient for our analysis to treat $\omega=O(\varepsilon^2)$, which we shall see represents an important distinguished limit of the system.

At $O(1)$, we obtain the leading-order system

$$0=dA_{0XX}+\lambda(1+rf(s(t),t))A_0-\gamma I_0 \tag{4.11a}$$

$$0=I_{0XX}+A_0-I_0. \tag{4.11b}$$

Since we are analysing the system near the Turing bifurcation, we seek the degenerate solution near $x=s(t)$, the position of which is to be determined.

Since σ and t effectively act as parameters in (4.11), analysis of the linear system (4.11) proceeds in a similar manner to a classic linear stability analysis for Turing patterning in a homogeneous environment. To this end, the position of the moving bifurcation $x=s(t)$ is defined implicitly through the relationship

$$f(s(t),t)=F_c, \tag{4.12}$$

for constant F_c to be determined as part of our analysis. The value that F_c takes at the onset of bifurcation will be the same as the value it would take in the scenario of a homogeneous environment (as recently shown more broadly in [11] for spatially varying environments).

Given (4.12), we write (4.11) as

$$\mathbf{D}\boldsymbol{A}_{0XX}+\mathbf{J}\boldsymbol{A}_0=0, \tag{4.13a}$$

where

$$\mathbf{D}=\begin{pmatrix}d & 0\\ 0 & 1\end{pmatrix}\quad\text{and}\quad\mathbf{J}=\begin{pmatrix}\lambda(1+rF_c) & -\gamma\\ 1 & -1\end{pmatrix}. \tag{4.13b}$$

The onset of the Turing bifurcation is then given by the criteria (e.g. [41])

$$[\mathrm{Tr}(\mathbf{D}^{-1}\mathbf{J})]^2=4\det[\mathbf{D}^{-1}\mathbf{J}],\quad \mathrm{Tr}[\mathbf{D}^{-1}\mathbf{J}]>0, \tag{4.14}$$

which combine to yield the following result for F_c:

$$F_c:=\frac{2\sqrt{\gamma d}-d-\lambda}{\lambda r}. \tag{4.15}$$

The result (4.15) allows us to write $\mathbf{J}$ in (4.13*b*) as

$$\mathbf{J}=\begin{pmatrix}2\sqrt{\gamma d}-d & -\gamma\\ 1 & -1\end{pmatrix}. \tag{4.16}$$

The remaining task at this order is to solve the system (4.13). In the standard manner, we look for a real solution proportional to $\mathrm{e}^{\mathrm{i}k_cX}$, where k_c is the (as-of-yet unknown) wavelength of

the patterned solution at the onset of bifurcation. Using this form of the solution, we see that k_c^2 corresponds to the *repeated* eigenvalues of $\mathbf{D}^{-1}\mathbf{J}$ at the onset of bifurcation, and hence that

$$k_c^2 := \sqrt{\frac{\gamma}{d}} - 1, \tag{4.17}$$

noting that $k_c^2 > 0$ for Turing patterning to be possible. Hence, the system (4.13) is solved by

$$\boldsymbol{A}_0 = \begin{pmatrix} \sqrt{\gamma} \\ \sqrt{d} \end{pmatrix} B(\sigma, t)\cos(k_c X + \psi), \tag{4.18}$$

where $(\sqrt{\gamma}, \sqrt{d})^\intercal$ is the right eigenvector of $\mathbf{D}^{-1}\mathbf{J}$, and the slowly varying amplitude B satisfies some governing equation that must be derived at higher asymptotic orders via our weakly nonlinear analysis. The derivation of this governing equation is the goal of our remaining analysis. Finally, we note that ψ is some phase shift that would have to be obtained via matching with a nonlinear outer solution. We note that knowledge of ψ is not required to capture the emergent amplitude nor frequency of patterning, since it only represents a translational shift in the patterning.

The $O(\varepsilon^{1/2})$ terms in (4.9) yield

$$\mathbf{D}\boldsymbol{A}_{1XX} + \mathbf{J}\boldsymbol{A}_1 = -2\mathbf{D}\boldsymbol{A}_{0X\sigma}. \tag{4.19}$$

Since the right-hand side of (4.19) is orthogonal to the left-eigenvector of the linear operator, we do not have enough information to impose a meaningful solvability condition at this order. Hence we must proceed to the next order to yield a governing equation for B. Nevertheless, we must still solve (4.19) in terms of $\boldsymbol{A}_0$, since the solvability condition we will derive at $O(\varepsilon)$ requires information about $\boldsymbol{A}_1$.

Using the solution (4.18), we see that the particular integral of (4.19) will be proportional to $\sin(k_c X + \psi)$. Looking for a particular integral in this form, we find that

$$\boldsymbol{A}_1 = -\frac{2k_c d}{\sqrt{\gamma}} B_\sigma \begin{pmatrix} 0 \\ 1 \end{pmatrix} \sin(k_c X + \psi) + B_1(\sigma, t)\cos(k_c X + \psi_1), \tag{4.20}$$

where the first term on the right-hand side is the particular integral of (4.19), and the second term on the right-hand side is the complementary function. B_1 is an undetermined function of σ and t, and ψ_1 is a constant that would be determined through matching at higher orders. We will not calculate either of these, since neither are required for our overarching goal: to derive a governing equation for B. This remains our objective, and to achieve this we proceed to the next asymptotic order.

The $O(\varepsilon)$ terms in (4.9) yield

$$\mathbf{D}\boldsymbol{A}_{2XX} + \mathbf{J}\boldsymbol{A}_2 = -\frac{\omega \dot{s}}{\varepsilon^2}\boldsymbol{A}_{0\sigma} + \begin{pmatrix} A_0^3 - \lambda r \sigma f_x(s(t), t) A_0 \\ 0 \end{pmatrix} - 2\mathbf{D}\boldsymbol{A}_{1X\sigma} - \mathbf{D}\boldsymbol{A}_{0\sigma\sigma}. \tag{4.21}$$

We can obtain the governing equation we seek for B by imposing a solvability condition on (4.21). To do this, we left-multiply the system (4.21) by its left-eigenvector (adjoint) solution $(1/\sqrt{d}, -\sqrt{\gamma})\cos(k_c X + \psi)$ and integrate over a single period in X, e.g. from $X = 0$ to $2\pi/k_c$. This procedure yields the following governing equation for B:

$$4d\left(1 - \sqrt{\frac{d}{\gamma}}\right) B_{\sigma\sigma} + \frac{\omega \dot{s}(1-d)}{\varepsilon^2} B_\sigma + \lambda r f_x(s(t), t)\sigma B - \frac{3\gamma}{4} B^3 = 0. \tag{4.22}$$

Finally, we note that we can rescale (4.22) into the normal form we give in (A 3) through the scalings

$$B = \frac{2(\lambda r f_x(s(t), t))^{1/3}\left(4d(1 - \sqrt{d/\gamma})\right)^{1/6}}{\sqrt{3\gamma}} y, \quad \sigma = \left(\frac{4d\left(1 - \sqrt{d/\gamma}\right)}{\lambda r f_x(s(t), t)}\right)^{1/3} z, \tag{4.23a}$$

with

$$\Gamma(t) := \frac{\omega \dot{s}(1-d)}{\varepsilon^2(\lambda r f_x(s(t),t))^{1/3}\left[4d(1-\sqrt{d/\gamma})\right]^{2/3}}. \tag{4.23b}$$

(ii) Spatio-temporal parameter oscillations

We now consider the case of spatio-temporal parameter oscillations, i.e. where the moving bifurcation can turn around. This is of particular interest in determining whether patterning persists dynamically even when an equilibrium analysis might suggest the repeated emergence and disappearance of a bifurcation at the edge of the domain. To analyse and quantify this effect, we scale into the region close to a generic fixed point $x = x^*$, around the time $t = t^*$ at which the bifurcation reaches this point. That is, t^* is defined implicitly through $f(x^*, t^*) = F_c$. We will later use this result to consider the potential persistence of a pattern-forming bifurcation at the edge of the domain.

We are specifically interested in the critical slowing down region where delayed effects dominate. We therefore use the new length, time and concentration scalings

$$\bar{X} = \frac{x - x^*}{\varepsilon^{3/2}}, \quad \bar{\sigma} = \frac{x - x^*}{\sqrt{\omega}}, \quad \bar{T} = \frac{t - t^*}{\sqrt{\omega}} \quad \text{and} \quad (\bar{A}, \bar{I}) = \frac{\omega^{1/4}}{\varepsilon^{1/2}}(A, I) \tag{4.24}$$

motivated by the fast wavelength scaling for X in (4.8), and the time, space and concentration scalings in (3.21).

After applying the scalings (4.24), the resulting analysis is very similar to that in the previous subsection, so we omit it for brevity. This analysis yields the general leading-order solution

$$\begin{pmatrix} \bar{A} \\ \bar{I} \end{pmatrix} \sim \frac{2(1-d)^{1/2}}{\sqrt{3\gamma}} \begin{pmatrix} \sqrt{\gamma} \\ \sqrt{d} \end{pmatrix} \bar{B}(\bar{\sigma}, \bar{T}) \cos(k_c \bar{X} + \bar{\psi}), \tag{4.25}$$

where the constants pre-multiplying this solution are added for notional convenience in presenting the following amplitude equation satisfied by the slowly varying amplitude $\bar{B}$:

$$\frac{\partial \bar{B}}{\partial \bar{T}} = \frac{4d\varepsilon^3}{\omega^{3/2}(1-d)}\left(1 - \sqrt{\frac{d}{\gamma}}\right)\frac{\partial^2 \bar{B}}{\partial \bar{\sigma}^2} + \bar{f}(\bar{\sigma}, \bar{T})\bar{B} - \bar{B}^3 = 0, \tag{4.26a}$$

where

$$\bar{f}(\bar{\sigma}, \bar{T}) := \frac{\lambda r}{1-d}\frac{f(x^* + \sqrt{\omega}\bar{\sigma}, t^* + \sqrt{\omega}\bar{T}) - F_c}{\sqrt{\omega}}, \tag{4.26b}$$

noting that F_c is defined in (4.15). Then, we see that if $\varepsilon \ll \omega^{1/2}$, the system (4.26) reduces to (3.18), which has solution (3.20). Hence, for a specified function f, we can calculate the value of $\bar{B}$ through the general solution (3.20). Moreover, for finite domains $x \in (0, 1)$, if we apply this analysis at the boundary $x = 1$,[2] we can calculate the critical oscillation period for which patterns persist (i.e. remain above a specified critical value) via simple one-dimensional root finding (see electronic supplementary material, figure S1).

5. Biological examples: results and implications

So far, we have analytically studied two biological pattern-forming systems: digit formation in the embryo in §4 and bacterial quorum sensing (QS) in the electronic supplementary material. Our modelling assumptions and the governing equations for each system are given at the beginning of §4 (Turing patterns) and the electronic supplementary material (QS); corresponding schematic diagrams are given in figures 2*a* and 3*a*, respectively. In both systems, we have derived results that quantify the dynamical and spatial effects of spatio-temporal pre-pattern morphogen variations. In this section, we link the analytical results in §4 and the electronic supplementary

[2]Assuming that our analysis holds near a boundary, which should hold unless the amplitude varies rapidly, i.e. unless the system exhibits a boundary layer near $x = 1$.

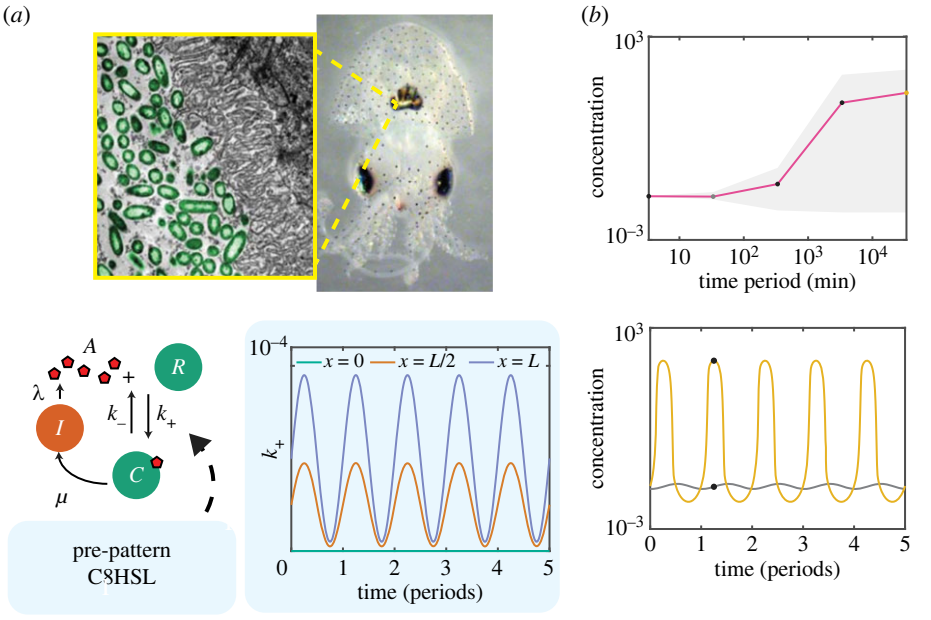

Figure 3. Effect of spatio-temporal morphogen variations on bacterial quorum sensing in a small biofilm or cell population. (*a*) We model quorum sensing in *V. fischeri*, which causes bioluminescence in the Hawaiian bobtail squid (top; images adapted from [42], with permission). We model the LuxR system, in which an autoinducer, 3OC6HSL, promotes its own synthesis by binding with a protein, LuxR, to form a transcription factor (bottom left). The binding parameter k_+ is modulated by competitive binding with a second autoinducer, C8HSL. Bottom right: the parameter k_+ ($\text{nM}^{-1}\,\text{s}^{-1}$) throughout the spatio-temporal oscillations (S2.4) (see also electronic supplementary material, movie S2). (*b*) Top: effect of the time period $\tilde{\tau}$ of the spatio-temporal oscillations in C8HSL on the mean 3OC6HSL concentration (line), and the range of 3OC6HSL concentration (grey area) during the oscillations. Bottom: oscillations in 3OC6HSL concentration, for fast ($\tilde{\tau} \approx 30$ min) and slow ($\tilde{\tau} \approx 3 \times 10^4$ min) oscillations in C8HSL. For oscillations that are filtered out, the system remains at low 3OC6HSL concentration. For oscillations that are not filtered out, the cell population fills with 3OC6HSL during the oscillation (see electronic supplementary material, movie S2). Concentrations in the figure are scaled by the quorum sensing activation threshold of 5 nM [13].

material to the robustness of biological pattern formation in pre-pattern morphogen variations. We also supplement the analytical results with the results of two-dimensional simulations of the governing equations of each system in the finite-element computational software COMSOL Multiphysics.

We begin by assuming for simplicity that pre-pattern morphogen variations act like a 'travelling wave' of the form (4.4). Our analysis in §4 and the electronic supplementary material shows that in this scenario, the governing equations of both biological systems reduce to the weakly nonlinear normal forms (2.6*a*) or (A 3). The pre-pattern morphogen variations are then encapsulated in two parameters, $\Lambda(t)$ and $\chi(t)$, defined through the ratio $\Gamma(t) := \chi/\Lambda^{2/3}$ in (4.23*b*) for the digit formation application and in (S2.27) in the electronic supplementary material for the QS application. Once $\Lambda(t)$ and $\chi(t)$ are calculated, the dynamics of the system are classified through the general parameter space shown in figure 1*c*. The parameter space contains three regions in which we predict qualitatively different solution behaviour (§3); we have named them Region A (reaction-dominated; quasi-steady), Region B (critical slowing down) and Region C (diffusively enhanced; quasi-steady). These results demonstrate that both of the paradigmatic pattern-forming systems considered here are subject to universal regimes that we have identified, which is a consequence of their bifurcation structures.

To understand the biological implications of the solution regimes in figure 1*c*, we now apply our analytical results to identify which regimes are most relevant to each biological system, and to quantify the dynamics of patterning in those regimes. First, we focus on the effects of pre-pattern morphogen variations that occur over physiological timescales. We use physiologically relevant values of the parameters in both systems (electronic supplementary material, tables S1 and S2), with the timescale of variation $\tilde{\tau}$ in the pre-pattern morphogen 'travelling wave' (4.4) corresponding to the relevant growth timescale; this is in line with experimental evidence that suggests physiological changes to patterning in each system are induced by growth [18,20,43]. Our analysis predicts that for such parameters, each system sits in Region C of parameter space (diffusively enhanced patterning; see figure 1*c*). In Region C, dynamics are quasi-steady, so we would expect both systems to respond promptly to temporal changes in morphogens that occur over physiological timescales. Also in Region C, patterning is 'enhanced' through diffusion so that areas ahead of the pre-pattern morphogen 'travelling wave' become patterned (a precise summary of this effect is given in §3). We predict significant quantitative differences in the spatial extent of patterning between the two systems because of this effect. In the Turing system, the diffusive enhancement to patterning is less than 10% of the size of the domain (see electronic supplementary material, table S1)—patterning would be expected to be controlled relatively locally by the concentration of the pre-pattern morphogen Fgf. This prediction is in line with recent analyses of Turing systems in steady pre-pattern morphogen gradients, in which patterning was found to be controlled relatively locally in space [11]. By contrast, our analysis predicts that diffusive enhancement to patterning is much stronger in the bacterial QS system. We find that diffusive enhancement causes the patterned (or QS-activated) region to be larger than the size of the population (electronic supplementary material, table S2)—any local activation in QS caused by changes over a growth timescale would be expected to cause the entire population to activate. This would benefit the population by ensuring all cells commit together to a multicellular program of gene expression, as was recently found in fluid flows [13]. These results suggest that biological pattern-forming systems can tune via diffusion the extent of patterning.

With the aim of understanding robustness, we next investigate the effect of spatio-temporal morphogen variations that occur faster than growth. Interestingly, by reducing the timescale of variation $\tilde{\tau}$ in the pre-pattern morphogen 'travelling wave' (4.4), we find that each system transitions to Region B (critical slowing down) of parameter space at a critical value of $\tilde{\tau}$ (electronic supplementary material, tables S1 and S2). In Region B, a bifurcation-associated emergent timescale slows the system dynamics (see §3)—this suggests that both systems may be slow to respond to pre-pattern morphogen variations that happen over timescales that are not physiological. To investigate this further, we now consider oscillatory pre-pattern morphogen variations of the form (4.3) in each system (see electronic supplementary material, movies S1 and S2); in a quasi-steady system, we would expect to see periodic cycles in which patterning switches on and off. However, our analytical results show that in this scenario, for both pitchfork and transcritical bifurcations, there is a critical oscillation timescale—oscillations that occur faster than this timescale are predicted to be 'filtered out' because of the critical slowing down (see §4 and electronic supplementary material). Our simulations confirm this finding: for pre-pattern morphogen oscillations that occur faster than a critical timescale, we find that both biological systems remain stuck in the initial patterned or unpatterned state (figures 2*c*,*d* and 3*b*; electronic supplementary material, movies S1 and S2). We calculate the critical timescale to be around 3–10 hours, depending on the kinetic parameters in each system (figures 2*c*; and 3*b*; electronic supplementary material, figure S1)—surprisingly, this is a few hours faster than the timescale of growth in both systems (electronic supplementary material, tables S1 and S2). Therefore, we expect changes in the pre-pattern morphogen concentration to be ignored if they occur much faster than a growth timescale, allowing the system to avoid repeated cycles of complete removal of patterning (figures 2*d* and 3*b*; electronic supplementary material, movies S1 and S2). Remarkably, this suggests that the gene-regulatory parameters in each biological system are tuned such that each system is robust to non-physiological variations in pre-pattern morphogens.

6. Discussion and conclusion

This study concerns biological pattern-forming systems with spatio-temporal variations in pre-pattern morphogens; we assume that the pre-pattern morphogens affect the kinetics of the underlying gene-regulatory network. Mathematically, this corresponds to variations in the parameters of the governing reaction–diffusion equations; the onset (or offset) of pattern formation is induced when variations cause the system to transition through a bifurcation. Our analysis of such systems demonstrates how the dynamics of biological pattern formation in pre-pattern morphogen variations can be classified and quantified in terms of universal solution regimes that we have identified. Each solution regime displays qualitatively different dynamics—the regime in which a biological system sits depends on the gene-regulatory kinetics, and on the timescale of the pre-pattern morphogen variations.

This presents the intriguing possibility that, with the appropriate gene-regulatory kinetics, a biological system could take advantage of different solution regimes in different situations. Surprisingly, our results indeed suggest that in both of the biological systems that we have studied, the system transitions into the 'critical slowing down' regime if variations in pre-pattern morphogens become much faster than growth. In this 'critical slowing down' regime, the onset (or offset) of pattern formation occurs over a new, longer, timescale that emerges because of the presence of a bifurcation in the system. We predict that this allows the biological systems to 'filter out' non-physiological oscillations in pre-pattern morphogens. Overall, our results suggest that dynamic delaying effects can manifest from supercritical bifurcations in reaction–diffusion systems, which are associated with the onset of patterning, providing an effective hysteresis and inherent robustness to biological systems. These results complement recent work that highlights the benefit of subcritical transitions for a similar purpose [44].

In principle, any pattern-forming system that undergoes a transcritical or supercritical pitchfork bifurcation can be analysed using our asymptotic framework and plotted on the parameter space that our analysis has produced (figure 1*c*). We expect that our results can be readily extended to wider classes of systems with continuous transitions, such as those with supercritical Hopf bifurcations in their underlying governing equations. While the 'early-time' analogues of our off-to-on results may be extended to the discontinuous transitions that typify subcritical bifurcations (which are likely to arise in multistable systems), a comprehensive analysis of subcritical bifurcations would pose additional technical challenges due to the global nature of the solution structure. Nevertheless, the general principles that we have investigated here and their implications for robustness would still hold for discontinuous transitions; the presence of any bifurcation will impart additional intermediate timescales for pattern forming systems, and this will act as a low-pass filter for spatio-temporal variations. Our general framework complements recent work on pattern formation in various systems of equations with spatio-temporally varying parameters (e.g. [11,45–53]) and on the effect of critical slowing down in a range of contexts [54,55]. Furthermore, our classification of the dynamics of gene-regulatory network architectures via their low-dimensional mathematical structure (i.e. bifurcations) complements recent work on dimensionality reduction of systems without spatio-temporal heterogeneity [32,56,57] and systems transitioning from a dynamic to a static regime [25].

We have applied our results to two specific biological pattern-forming systems. In modelling these systems, we have performed significant simplifications for clarity and generality. In particular, we have not modelled the effect of stochastic noise in pre-pattern morphogen concentrations, which we expect to have effects that are not captured by our analysis [58,59]. Furthermore, our models are effective macroscopic representations of microscopic processes, and the process of coarse-graining the microscopic dynamics to obtain effective macroscopic dynamics is often not trivial [60].

To conclude, we have presented a general framework that classifies and quantifies the dynamic response of pattern-forming systems to spatio-temporal variations in their parameters. We have applied our framework to simple models of two biological pattern-forming systems, each with

variations in a pre-pattern morphogen that affects kinetic parameters: digit formation via Turing patterns, and bacterial quorum sensing. Our theory predicts that both systems filter out spatio-temporal morphogen variations that occur much faster than growth. We demonstrate that the type of bifurcation in the system, which is determined by the gene-regulatory network, controls emergent patterning dynamics and structure. Predictions such as these are testable in newly developed systems that allow spatio-temporal control over gene-expression and the external environment, such as synthetic model organisms [61], organoids [62] and microfluidic devices [27]. Owing to the generality of the canonical equations that we have analysed, our theoretical framework is extendable to a wide class of pattern-forming systems.

Data accessibility. The code that was used to perform the simulations in this paper is available at: https://github.com/philip-pearce/quorum-flow/. All data is provided in the paper and in the electronic supplementary material [63].

Authors' contributions. M.P.D. and P.P. designed research, performed research, analyzed data, and wrote the paper. Both authors gave final approval for publication and agreed to be held accountable for the work performed therein.

Conflict of interest declaration. We declare we have no competing interests.

Acknowledgements. We thank Zena Hadjivasiliou and Jake Cornwall Scoones for helpful discussions, and Eric Stabb for assistance with figure 3*a*. We would also like to acknowledge Andrew Krause for helpful comments on the text.

Funding. M.P.D. is supported by the UK Engineering and Physical Sciences Research Council (grant no. EP/W032317/1). P.P. is supported by a UKRI Future Leaders Fellowship (MR/V022385/1).

Appendix A. Perfect bifurcations

For a perfect bifurcation, $a = 0$ in (2.1). Although this can be treated through appropriate rescalings and limits of the imperfect case, the process is clearer if we simply rescale differently from the outset. Hence, we introduce the scaled variables $z(x,t) = O(1)$ and $y(z,t) = O(1)$ via

$$x = s(t) + \left(\frac{D}{\eta}\right)^{1/3} z \quad \text{and} \quad A = \left(\frac{D^{1/3}\eta^{2/3}}{\varepsilon}\right)^{1/(n-1)} y. \tag{A 1}$$

Noting that $k(x,t) \sim D^{1/3}\eta^{2/3}z$, we obtain the transformed system

$$\frac{\omega}{D^{1/3}\eta^{2/3}}\left(\frac{\partial y}{\partial t} + \frac{\dot{\eta}z}{3\eta}\frac{\partial y}{\partial z} - \frac{\eta^{1/3}\dot{s}}{D^{1/3}}\frac{\partial y}{\partial z}\right) = \frac{\partial^2 y}{\partial z^2} + zy - y^n. \tag{A 2}$$

As before, but now exploiting $D \ll 1$, for non-degenerate cases the first two terms in the brackets on the left-hand side are asymptotically sub-dominant to the third. Consistently retaining all remaining terms represents a distinguished asymptotic limit

$$0 = \frac{\partial^2 y}{\partial z^2} + \Gamma(t)\frac{\partial y}{\partial z} + zy - y^n, \quad \text{where } \Gamma(t) := \frac{\chi}{\Lambda^{2/3}} = \frac{\omega\dot{s}}{D^{2/3}\eta^{1/3}}, \tag{A 3}$$

where Λ and χ are defined in (2.6*b*), and $\Gamma \in (-\infty, \infty)$ quantifies the importance of spatio-temporal variations in comparison to diffusion.

The appropriate far-field conditions can be obtained by matching into the outer quasi-steady solutions. Although there is some subtlety involved in matching into the unpatterned region in general for perfect bifurcations, in terms of what is required for our purposes we may close the normal form (A 3) by writing our matching conditions as

$$y \to 0 \text{ as } z \to -\infty, \quad y \sim z^{1/(n-1)} \text{ as } z \to +\infty. \tag{A 4}$$

The normal form for a perfect pitchfork is therefore defined by (A 3) and (A 4) with $n = 3$. We now note the differences in the monotonic analysis for perfect bifurcations.

(a) Region A

Since positive feedback dominates and balances base production in Region A, this region is not relevant in the case of a perfect bifurcation.

(b) Region B

The Region B sublimit is equivalent to $\Gamma \gg 1$ in (A 3) and (A 4). Then, the scalings $z \sim \Gamma^{1/2}$ and $y \sim \Gamma^{1/4}$ result in (3.2) at leading order, so the appropriate solution is the equivalent of (3.4):

$$y = \Gamma^{1/4} \frac{\exp(-z^2/2\Gamma)}{\pi^{1/4}\sqrt{\operatorname{erfc} z/\sqrt{\Gamma}}}. \tag{A 5}$$

However, for a perfect bifurcation, there is no base production to mediate the exponential decay in the far-field as $z \to -\infty$. Hence, dependent on the precise far-field matching conditions (which will depend on the specific system and its history), it is possible for diffusive effects to reassert themselves in the far-field. That is, there is an additional feasible asymptotic region in this sublimit when $-z = O(\Gamma^2)$. In this region, y is exponentially small and the appropriate version of (A 3) is its linearization, so that saturation effects can be ignored. A WKBJ analysis of the linearization of (A 3) (matching appropriately with (A 5)) yields the solution

$$y \sim \Gamma^{1/4} \frac{\exp[\Gamma^3 \phi(z/\Gamma^2)]}{(4\pi(1 - 4z/\Gamma^2))^{1/4}}, \quad \phi(\zeta) = -\frac{1}{12}(6\zeta - 1 + (1 - 4\zeta)^{3/2}). \tag{A 6}$$

Hence, the extent of the transition region for the perfect case will depend on how small one requires y to be when defining the position of the dynamic bifurcation. Our results allow for straightforward calculation of the extent once this critical size is defined.

(c) Region C

The Region C limit is equivalent to $\Gamma \ll 1$ in (A 3) and (A 4). In this case, the leading-order version of (A 3), (A 4) is exactly (3.11) with far-field decay as $\zeta \to -\infty$. Since the leading-order system in this limit is a regular sublimit of (A 3), we can use the scaling (A 1) to infer that the extent of the transition region in this case will be $x - s(t) = O((D/\eta)^{1/3})$, and that the behaviour of y as $z \to -\infty$ will be $y \sim c_R\,\mathrm{Ai}(-z)$ for some constant $c_R = O(1)$.

Appendix B. Asymptotic analysis of imperfect transcritical bifurcations

(a) Travelling-wave-like motion for off-to-on transcritical bifurcations

In this appendix, we consider imperfect transcritical pitchfork bifurcations, where the bifurcation moves unidirectionally from the patterned to the unpatterned state (i.e. off-to-on). The transcritical nature corresponds to the governing equation (2.6) with $n = 2$, and far-field conditions (2.7). The 'off-to-on' nature corresponds to $\chi < 0$. We now analyze the distinguished asymptotic limits of the ODE (2.6) with boundary conditions (2.7). This will allow us to derive analytic leading-order solutions, and subsequently to quantify the effect of dynamically crossing the bifurcation. While the analytic results we obtain for Y and Z^* are specific to the case $\chi < 0$, the asymptotic order of scalings for Z^* will be of the same order for $\chi > 0$. We proceed by analysing each region in increasing order of complexity.

(i) Positive feedback dominates: Region A

In Region A, $\Lambda, |\chi| \ll 1$ and positive feedback dominates. In this case, the ODE (2.6) becomes quasi-steady

$$1 + ZY - Y^2 = 0, \tag{B 1}$$

and is solved by

$$Y = \frac{Z + \sqrt{Z^2 + 4}}{2}. \tag{B 2}$$

Therefore, $Y(0) = 1$ so $Z^* = 0$. Hence, in Region A, the bifurcation takes its equilibrium (quasi-steady) position, and the patterning is spatially local and quasi-steady.

(ii) Spatio-temporal variations dominate: Region B

Region B occurs when $|\chi| \gg 1$ and $\Lambda/|\chi|^{3/2} \ll 1$. Here, spatio-temporal changes in the parameters dominate and delaying effects become important. In this region, there are sharp transitions between the unpatterned and patterned parts, separated by $Z = Z_c$.

To summarize the asymptotic structure, in Region B the interesting behaviour occurs over the lengthscale $Z = O(\sqrt{|\chi|})$, so we scale into a new independent variable $\sigma = Z/\sqrt{|\chi|}$. The solution is then split into two asymptotic regions separated by the point $\sigma = \sigma_c := Z_c/\sqrt{|\chi|}$. The determination of σ_c is a key goal of our analysis. The unpatterned region corresponds to $\sigma < \sigma_c$ and the patterned region corresponds to $\sigma > \sigma_c$. The solution is smaller in the unpatterned region, with the scaling $Y = Y_L/\sqrt{|\chi|}$, and larger in the patterned region, with the scaling $Y = \sqrt{|\chi|}Y_R$.

Here, information travels in the same direction as the pattern transition i.e. from the unpatterned state to the patterned state (off-to-on). As such, our analysis starts in the unpatterned state, where $\sigma < \sigma_c$. Using the scalings noted above, the leading-order scaled version of the ODE system (2.6), (2.7) in the unpatterned state ($\sigma < \sigma_c$) is

$$\frac{\partial Y_L}{\partial \sigma} = 1 + \sigma Y_L, \quad Y_L \sim -\frac{1}{\sigma} \quad \text{as } \sigma \to -\infty, \tag{B 3}$$

which is solved by

$$Y_L = \sqrt{\frac{\pi}{2}}\left(1 + \operatorname{erf}\frac{\sigma}{\sqrt{2}}\right)\exp\left(\frac{\sigma^2}{2}\right). \tag{B 4}$$

Given the relative scalings of Y in the unpatterned and patterned regions, we can determine σ_c by calculating when $Y_L = O(|\chi|)$. Since (B 4) yields the far-field result

$$Y_L \sim \sqrt{2\pi}\,\mathrm{e}^{\sigma^2/2} \quad \text{as } \sigma \to \infty, \tag{B 5}$$

it is straightforward to note that $\sigma_c \sim \sqrt{2\log|\chi|}$.

Using the scalings noted above, the leading-order scaled version of the ODE system (2.6) and (2.7) in the patterned state ($\sigma > \sigma_c$) is

$$\frac{\partial Y_R}{\partial \sigma} = \sigma Y_R - Y_R^2, \tag{B 6}$$

closed by matching appropriately with (B 4). The patterned system (B 6) is solved by

$$Y_R = \frac{\exp(\sigma^2/2)}{k_\mathrm{B} + \int_0^\sigma \exp(u^2/2)\,\mathrm{d}u}, \quad k_\mathrm{B} = \frac{|\chi|}{\sqrt{2\pi}}, \tag{B 7}$$

where k_B is the constant determined by matching with (B 4). The matching procedure involves tracking the exponentially growing term (B 5) within a logarithmic transition region where $Y_L = O(|\chi|)$. Specifically, an intermediate transition region where $\sigma - \sigma_c = O(1/\sigma_c)$.

Finally, we calculate the dynamic position of the bifurcation $Z = Z^*$ at which $Y(Z^*) = 1$. Our scalings give $Z^* = \sqrt{|\chi|}\sigma^*$ where $Y_L(\sigma^*) = \sqrt{|\chi|}$. From (B 4), this occurs when $\sigma^* \sim \sqrt{\log|\chi|}$, and hence we obtain the following asymptotic result for the dynamic position of the bifurcation:

$$Z^* \sim \sqrt{|\chi|\log|\chi|} \quad \text{for } |\chi| \gg 1 \text{ and } \Lambda/|\chi|^{3/2} \ll 1 \quad \text{(Region B)}. \tag{B 8}$$

(iii) Diffusion dominates: Region C

Region C occurs when $\Lambda \gg 1$ and $\Lambda/|\chi|^{3/2} \gg 1$. Here, diffusive effects dominate. As before, there are sharp transitions between the unpatterned and patterned parts of the transition region separated by $Z = Z_c$.

To summarize the asymptotic structure, the interesting behaviour in Region C occurs over the lengthscale $Z = O(\Lambda^{1/3})$, so we scale into a new independent variable $\zeta = Z/\Lambda^{1/3}$. The solution is again split into two asymptotic regions, matched via an intermediate transition region. The two main asymptotic regions are separated by the point $\zeta = \zeta_c := Z_c/\Lambda^{1/3}$. The determination of ζ_c is a key goal of our analysis. The unpatterned region corresponds to $\zeta < \zeta_c$ and the patterned region to $\zeta > \zeta_c$. The solution is smaller in the unpatterned region, with the scaling $Y = W_L/\Lambda^{1/3}$, and larger in the patterned region, with the scaling $Y = \Lambda^{1/3} W_R$.

Using these scalings, the leading-order versions of (2.6) and (2.7) in the unpatterned state ($\zeta < \zeta_c$) are

$$\frac{\partial^2 W_L}{\partial \zeta^2} + 1 + \zeta W_L = 0, \quad W_L \sim -\frac{1}{\zeta} \text{ as } \zeta \to -\infty. \tag{B 9}$$

This is equivalent to (3.12), and hence solved by (3.13), where c_L is to be determined through matching with the patterned region.

In the patterned state $\zeta > \zeta_c$, the leading-order scaled version of the ODE (2.6) and (2.7) is

$$\frac{\partial^2 W_R}{\partial \zeta^2} + \zeta W_R - W_R^2 = 0, \quad W_R \sim \zeta \text{ as } \zeta \to \infty. \tag{B 10}$$

Given the relative scalings of Y in each asymptotic region, the position $\zeta = \zeta_c$ can be deduced by calculating when $W_R = O(\Lambda^{-2/3})$. Similarly, the dynamic position of the bifurcation $Z^* = \Lambda^{1/3}\zeta^*$ can be inferred through the relationship $Y(Z^*) = 1$, and hence when $W_R(\zeta^*) = \Lambda^{-1/3}$. Hence, we require knowledge of the decaying behaviour of the nonlinear ODE (B 10) as we move towards the unpatterned far-field $\zeta \to -\infty$. Linearizing (B 10) around the far-field trivial solution and imposing decay results in the behaviour

$$W_R \sim c_R \,\mathrm{Ai}(-\zeta), \quad \text{as } \zeta \to -\infty, \tag{B 11}$$

where $c_R = O(1)$ is a constant that can be determined by solving (B 10) numerically and imposing decaying behaviour as $\zeta \to -\infty$. Using the far-field behaviour of the Airy function, we find that $W_R = O(\Lambda^{-2/3})$ for $\zeta_c \sim -(\log \Lambda)^{2/3}$ and that $W_R(\zeta^*) = \Lambda^{-1/3}$ yields $\zeta^* \sim -(\log \sqrt{\Lambda})^{2/3}$, resulting in the following asymptotic result for the dynamic position of the bifurcation

$$Z^* \sim -\left(\frac{\Lambda \log^2 \Lambda}{2}\right)^{1/3} \quad \text{for } \Lambda \gg 1 \text{ and } \Lambda/|\chi|^{3/2} \gg 1 \quad \text{(Region C)}. \tag{B 12}$$

(b) Spatio-temporal oscillations for transcritical bifurcations

Here, we consider spatio-temporal oscillations for transcritical bifurcations going from unpatterned-patterned-unpatterned. This is the transcritical equivalent of §3b in the main text. We consider (2.1) with $n = 2$ and $a > 0$ (which will give an imperfect transcritical bifurcation):

$$\omega \frac{\partial A}{\partial t} = D \frac{\partial^2 A}{\partial x^2} + a + k(x,t)A - \varepsilon A^2. \tag{B 13}$$

We follow the main text analysis, and zoom into a region near the generic fixed point $x = x^*$, around the time $t = t^*$ defined through $k(x^*, t^*) = 0$. We are specifically interested in understanding when the system overcomes the forcing to pattern and remains unpatterned in the dynamic case, demonstrating intrinsic robustness. Therefore, we investigate when the critical slowing down effect of Region B can overcome this forcing before the system returns to the locally unpatterned state. That is, quantifying when the system is robust to temporary incursions into regimes that would appear to be unpatterned from a quasi-steady analysis.

We are specifically interested in understanding when forcing transitions from unpatterned-patterned-unpatterned resist patterning and remain unpatterned, so the key terms in (B 13) are the left-hand side and the second and third terms on the right-hand side. While we will formalize this intuitive dominant balance for the specific scenarios in which we are interested below, it is helpful to note that the relevant asymptotic scalings will reduce (B 13) to a leading-order equation of the form

$$\frac{\partial Y}{\partial T} = 1 + \bar{k}(X,T)Y, \quad Y \sim -\frac{1}{\bar{k}(X,T)} \text{ as } T \to -\infty, \tag{B 14}$$

for appropriately defined variables X, T, $Y(X,T)$ and function $\bar{k}(X,T)$. It is straightforward to derive the following solution of the linear ODE (B 14) in terms of $\bar{k}$:

$$Y(X,T) \sim \mathrm{e}^{\overline{K}(X,T)} \int_{-\infty}^{T} \mathrm{e}^{-\overline{K}(X,s)} \mathrm{d}s \quad \text{where } \overline{K}(X,T) := \int_{0}^{T} \bar{k}(X,s)\,\mathrm{d}s. \tag{B 15}$$

(c) Fixed away from the turning point

We first consider the case where $k_t(x^*,t^*) \neq 0$, where the appropriate inner equation scalings into the initially patterned region are

$$x = x^* + \sqrt{\omega}X, \quad t = t^* + \sqrt{\omega}T \quad \text{and} \quad A = \frac{a}{\sqrt{\omega}}Y. \tag{B 16}$$

These scalings turn (B 13) into

$$\frac{\partial Y}{\partial T} = \frac{\widehat{\Lambda}}{\widehat{\chi}^{3/2}} \frac{\partial^2 Y}{\partial X^2} + 1 + \bar{k}(X,T)Y - \frac{Y^2}{\widehat{\chi}}, \tag{B 17}$$

where we introduce the parameter groupings

$$\widehat{\Lambda} = \frac{D}{(a\varepsilon)^{3/2}} \quad \text{and} \quad \widehat{\chi} = \frac{\omega}{a\varepsilon}, \tag{B 18}$$

keeping similar notation as in (2.6*b*), and the function

$$\bar{k}(X,T) := \frac{k(x^* + \sqrt{\omega}X, t^* + \sqrt{\omega}T)}{\sqrt{\omega}}. \tag{B 19}$$

We note that $\bar{k} = O(1)$ since $k(x^*,t^*) = 0$. Moreover, while it is possible to replace the right-hand side of (B 19) with its linearization for many differentiable functions k, we retain its general form since we are specifically interested in oscillations in T. That is, we are specifically interested in $\bar{k}$ with turning points in T, and these will generally not be well-approximated by their linearizations.

The formal neglect of the diffusive and saturation terms in (B 17) correspond to the limits $\widehat{\chi} = \omega/(a\varepsilon) \gg 1$ and $\widehat{\Lambda}/\widehat{\chi}^{2/3} = D/\omega^{3/2} \ll 1$, directly analogous to the limits that took us into Region B previously. Moreover, these limits reduce (B 17) to (B 14), which is solved by (B 15).

For any specified oscillatory function $k(x,t)$ (and hence $\bar{k}(X,T)$), we can calculate when Y reaches a critical minimal value (specified by the particular problem being considered) via one-dimensional root finding of the analytic solution (B 15).

(d) Fixed at the turning point

We now consider the case where $k_t(x^*,t^*) = 0$ and $k_{tt}(x^*,t^*) < 0$, where the appropriate inner equation scalings are

$$x = x^* + \omega^{2/3}X, \quad t = t^* + \omega^{1/3}T \quad \text{and} \quad A = \frac{a}{\omega^{2/3}}Y. \tag{B 20}$$

These scalings turn (B 13) into

$$\frac{\partial Y}{\partial T} = \frac{\widehat{\Lambda}}{\tilde{\chi}^{3/2}} \frac{\partial^2 Y}{\partial X^2} + 1 + \tilde{k}(X,T)Y - \frac{Y^2}{\tilde{\chi}}, \tag{B 21}$$

where $\widehat{\Lambda}$ is defined in (B 18), and we introduce the following parameter grouping $\tilde{\chi}$ and function $\tilde{k}(X,T)$

$$\tilde{\chi} = \frac{\omega^{4/3}}{a\varepsilon} = \omega^{1/3}\widehat{\chi} \quad \text{and} \quad \tilde{k}(X,T) := \frac{k(x^* + \omega^{2/3}X, t^* + \omega^{1/3}T)}{\omega^{2/3}}, \tag{B 22}$$

where $\widehat{\chi}$ is defined in (B 18). The formal neglect of the diffusive and saturation terms in (B 21) correspond to the limits $\tilde{\chi} = \omega^{4/3}/(a\varepsilon) \gg 1$ and $\widehat{\Lambda}/\tilde{\chi}^{3/2} = D/\omega^2 \ll 1$. If these constraints are satisfied, this limit reduces (B 21) to the system (B 14), which is solved by (B 15).

References

1. Maini PK, Woolley TE, Baker RE, Gaffney EA, Lee SS. 2012 Turing's model for biological pattern formation and the robustness problem. *Interface Focus* **2**, 487–496. (doi:10.1098/rsfs.2011.0113)
2. Alon U. 2019 *An introduction to systems biology*, 2nd edn. Boca Raton, FL: CRC Press and Chapman and Hall/CRC.
3. Vittadello ST, Leyshon T, Schnoerr D, Stumpf MPH. 2021 Turing pattern design principles and their robustness. *Phil. Trans. R. Soc. A* **379**, 20200272. (doi:10.1098/rsta.2020.0272)
4. Eldar A, Dorfman R, Weiss D, Ashe H, Shilo BZ, Barkai N. 2002 Robustness of the BMP morphogen gradient in Drosophila embryonic patterning. *Nature* **419**, 304–308. (doi:10.1038/nature01061)
5. Wartlick O, Mumcu P, Kicheva A, Bittig T, Seum C, Jülicher F, González-Gaitán M. 2011 Dynamics of Dpp signaling and proliferation control. *Science* **331**, 1154–1159. (doi:10.1126/science.1200037)
6. Mateus R, Holtzer L, Seum C, Hadjivasiliou Z, Dubois M, Jülicher F, Gonzalez-Gaitan M. 2020 BMP signaling gradient scaling in the zebrafish pectoral fin. *Cell Rep.* **30**, 4292–4302. (doi:10.1016/j.celrep.2020.03.024)
7. Scholes NS, Schnoerr D, Isalan M, Stumpf MP. 2019 A comprehensive network atlas reveals that Turing patterns are common but not robust. *Cell Syst.* **9**, 243–257. (doi:10.1016/j.cels.2019.07.007)
8. Green JBA, Sharpe J. 2015 Positional information and reaction-diffusion: two big ideas in developmental biology combine. *Development* **142**, 1203–1211. (doi:10.1242/dev.114991)
9. Jutras-Dubé L, El-Sherif E, François P. 2020 Geometric models for robust encoding of dynamical information into embryonic patterns. *eLife* **9**, 1–36. (doi:10.7554/eLife.55778)
10. Scoones JC, Hiscock TW. 2020 A dot-stripe Turing model of joint patterning in the tetrapod limb. *Development* **147**, dev183699. (doi:10.1242/dev.183699)
11. Krause AL, Klika V, Woolley TE, Gaffney EA. 2020 From one pattern into another: analysis of Turing patterns in heterogeneous domains via WKBJ. *J. R. Soc. Interface* **17**, 20190621. (doi:10.1098/rsif.2019.0621)
12. Barbier I, Perez-Carrasco R, Schaerli Y. 2020 Controlling spatiotemporal pattern formation in a concentration gradient with a synthetic toggle switch. *Mol. Syst. Biol.* **16**, e9361. (doi:10.15252/msb.20199361)
13. Dalwadi MP, Pearce P. 2021 Emergent robustness of bacterial quorum sensing in fluid flow. *Proc. Natl Acad. Sci. USA* **118**, e2022312118. (doi:10.1101/2020.10.23.352641)
14. Krause AL, Gaffney EA, Maini PK, Klika V. 2021 Modern perspectives on near-equilibrium analysis of Turing systems. *Phil. Trans. R. Soc. A* **379**, 20200268. (doi:10.1098/rsta.2020.0268)
15. Chakraborty P, Jolly MK, Roy U, Ghosh S. 2023 Spatio-temporal pattern formation due to host-circuit interplay in gene expression dynamics. *Chaos Solitons Fractals* **167**, 112995. (doi:10.1016/j.chaos.2022.112995)
16. Roy U, Singh D, Vincent N, Haritas CK, Jolly MK. 2022 Spatiotemporal patterning enabled by gene regulatory networks. *ACS Omega* **8**, 3713–3725. (doi:10.1021/acsomega.2c04581)
17. Turing AM. 1952 The chemical basis of morphogenesis. *Phil. Trans. R. Soc. Lond. B* **237**, 37–72. (doi:10.1098/rstb.1952.0012)
18. Sheth R, Marcon L, Bastida MF, Junco M, Quintana L, Dahn R, Kmita M, Sharpe J, Ros MA. 2012 *Hox* genes regulate digit patterning by controlling the wavelength of a Turing-type mechanism. *Science* **338**, 1476–1480. (doi:10.1126/science.1226804)
19. Paulsson J. 2004 Summing up the noise in gene networks. *Nature* **427**, 415–418. (doi:10.1038/nature02257)

20. Raspopovic J, Marcon L, Russo L, Sharpe J. 2014 Digit patterning is controlled by a Bmp-Sox9-Wnt Turing network modulated by morphogen gradients. *Science* **345**, 566–570. (doi:10.1126/science.1252960)
21. Ward JP, King JR, Koerber AJ, Croft JM, Sockett RE, Williams P. 2003 Early development and quorum sensing in bacterial biofilms. *J. Math. Biol.* **47**, 23–55. (doi:10.1007/s00285-002-0190-6)
22. Daniels R, Vanderleyden J, Michiels J. 2004 Quorum sensing and swarming migration in bacteria. *FEMS Microbiol. Rev.* **28**, 261–289. (doi:10.1016/j.femsre.2003.09.004)
23. Bhattacharyya S, Yeomans JM. 2021 Coupling Turing stripes to active flows. *Soft Matter* **17**, 10 716–10 722. (doi:10.1039/d1sm01218e)
24. Fulton T, Speiss K, Thomson L, Wang Y, Clark B, Hwang S, Paige B, Verd B, Steventon B. 2022 Cell rearrangement generates pattern emergence as a function of temporal morphogen exposure. *bioRxiv*. (doi:10.1101/2021.02.05.429898)
25. Wigbers MC, Tan TH, Brauns F, Liu J, Swartz SZ, Frey E, Fakhri N. 2021 A hierarchy of protein patterns robustly decodes cell shape information. *Nat. Phys.* **17**, 578–584. (doi:10.1038/s41567-021-01164-9)
26. Patel K, Rodriguez C, Stabb EV, Hagen SJ. 2020 Spatially propagating activation of quorum sensing in *Vibrio fischeri* and the transition to low population density. *Phys. Rev. E* **101**, 062421 (doi:10.1103/PhysRevE.101.062421)
27. Kim MK, Ingremeau F, Zhao A, Bassler BL, Stone HA. 2016 Local and global consequences of flow on bacterial quorum sensing. *Nat. Microbiol.* **1**, 15005. (doi:10.1038/nmicrobiol.2015.5)
28. Mukherjee S, Bassler BL. 2019 Bacterial quorum sensing in complex and dynamically changing environments. *Nat. Rev. Microbiol.* **17**, 371–382. (doi:10.1038/s41579-019-0186-5)
29. Pearce P *et al.* 2019 Flow-induced symmetry breaking in growing bacterial biofilms. *Phys. Rev. Lett.* **123**, 258101 (doi:10.1103/PhysRevLett.123.258101)
30. Brauns F, Halatek J, Frey E. 2020 Phase-space geometry of mass-conserving reaction-diffusion dynamics. *Phys. Rev. X* **10**, 041036 (doi:10.1103/PhysRevX.10.041036)
31. Woolley TE. 2022 Boundary conditions cause different generic bifurcation structures in Turing systems. *Bull. Math. Biol.* **84**, 101. (doi:10.1007/s11538-022-01055-x)
32. Sáez M, Blassberg R, Camacho-Aguilar E, Siggia ED, Rand DA, Briscoe J. 2021 Statistically derived geometrical landscapes capture principles of decision-making dynamics during cell fate transitions. *Cell Syst.* **13**, 12–28. (doi:10.1016/j.cels.2021.08.013)
33. Strogatz SH. 2015 *Nonlinear dynamics and chaos*. New York, NY: CRC Press.
34. Mandel P, Erneux T. 1987 The slow passage through a steady bifurcation: delay and memory effects. *J. Stat. Phys.* **48**, 1059–1070. (doi:10.1007/BF01009533)
35. Tredicce JR, Lippi GL, Mandel P, Charasse B, Chevalier A, Picqué B. 2004 Critical slowing down at a bifurcation. *Am. J. Phys.* **72**, 799–809. (doi:10.1119/1.1688783)
36. De Maesschalck P, Kaper TJ, Popović N. 2009 Canards and bifurcation delays of spatially homogeneous and inhomogeneous types in reaction-diffusion equations. *Adv. Differ. Equ.* **14**, 943–962. (doi:10.57262/ade/1355863335)
37. Tzou JC, Ward MJ, Kolokolnikov T. 2015 Slowly varying control parameters, delayed bifurcations, and the stability of spikes in reaction-diffusion systems. *Physica D* **290**, 24–43. (doi:10.1016/j.physd.2014.09.008)
38. Avitabile D, Desroches M, Veltz R, Wechselberger M. 2020 Local theory for spatio-temporal canards and delayed bifurcations. *SIAM J. Math. Anal.* **52**, 5703–5747. (doi:10.1137/19M1306610)
39. Olver FWJ *et al.* 2020 NIST digital library of mathematical functions. See http://dlmf.nist.gov/, Release 1.0.26 of 2020-03-15.
40. Visick KL, Stabb EV, Ruby EG. 2021 A lasting symbiosis: how *Vibrio fischeri* finds a squid partner and persists within its natural host. *Nat. Rev. Microbiol.* **19**, 654–665. (doi:10.1038/s41579-021-00557-0)
41. Murray JD. 2001 *Mathematical biology II: spatial models and biomedical applications*, vol. **3**. New York, NY: Springer.
42. Stabb EV. 2014 The *Vibrio fischeri—Euprymna scolopes* light organ symbiosis. In *The biology of Vibrios* , pp. 204–218. Washington, DC: ASM Press. (doi:10.1128/9781555815714.ch14)
43. Singh PK, Bartalomej S, Hartmann R, Jeckel H, Vidakovic L, Nadell CD, Drescher K. 2017 *Vibrio cholerae* combines individual and collective sensing to trigger biofilm dispersal. *Curr. Biol.* **27**, 3359–3366. (doi:10.1016/j.cub.2017.09.041)

44. Champneys AR, Al Saadi F, Breña-Medina VF, Grieneisen VA, Maree AF, Verschueren N, Wuyts B. 2021 Bistability, wave pinning and localisation in natural reaction–diffusion systems. *Physica D* **416**, 132735. (doi:10.1016/j.physd.2020.132735)
45. Page K, Maini PK, Monk NA. 2003 Pattern formation in spatially heterogeneous Turing reaction-diffusion models. *Physica D* **181**, 80–101. (doi:10.1016/S0167-2789(03)00068-X)
46. Page KM, Maini PK, Monk NA. 2005 Complex pattern formation in reaction-diffusion systems with spatially varying parameters. *Physica D* **202**, 95–115. (doi:10.1016/j.physd.2005.01.022)
47. Cuesta CM, King JR. 2010 Front propagation in a heterogeneous Fisher equation: the homogeneous case is non-generic. *Q. J. Mech. Appl. Math.* **63**, 521–571. (doi:10.1093/qjmam/hbq017)
48. Woolley TE, Krause AL, Gaffney EA. 2021 Bespoke Turing systems. *Bull. Math. Biol.* **83**, 41 (doi:10.1007/s11538-021-00870-y)
49. Goh R, Scheel A. 2018 Pattern-forming fronts in a Swift–Hohenberg equation with directional quenching—parallel and oblique stripes. *J. Lond. Math. Soc.* **98**, 104–128. (doi:10.1112/jlms.12122)
50. Rüdiger S, Nicola EM, Casademunt J, Kramer L. 2007 Theory of pattern forming systems under traveling-wave forcing. *Phys. Rep.* **447**, 73–111. (doi:10.1016/j.physrep.2007.02.017)
51. Liu Y, Maini PK, Baker RE. 2022 Control of diffusion-driven pattern formation behind a wave of competency. *Physica D* **438**, 133297. (doi:10.1016/j.physd.2022.133297)
52. Würthner L, Brauns F, Pawlik G, Halatek J, Kerssemakers J, Dekker C, Frey E. 2022 Bridging scales in a multiscale pattern-forming system. *Proc. Natl Acad. Sci. USA* **119**, e2206888119. (doi:10.1073/pnas.2206888119)
53. Goh R, Kaper TJ, Scheel A, Vo T. 2022 Fronts in the wake of a parameter ramp: slow passage through pitchfork and fold bifurcations. Preprint (https://arxiv.org/abs/2212.09131)
54. Gomez M, Moulton DE, Vella D. 2017 Critical slowing down in purely elastic 'snap-through' instabilities. *Nat. Phys.* **13**, 142–145. (doi:10.1038/nphys3915)
55. Liu M, Gomez M, Vella D. 2021 Delayed bifurcation in elastic snap-through instabilities. *J.Mech. Phys. Solids* **151**, 104386 (doi:10.1016/j.jmps.2021.104386)
56. Corson F, Siggia ED. 2012 Geometry, epistasis, and developmental patterning. *Proc. Natl Acad. Sci. USA* **109**, 5568–5575. (doi:10.1073/pnas.1201505109)
57. Rand DA, Raju A, Sáez M, Corson F, Siggia ED. 2021 Geometry of gene regulatory dynamics. *Proc. Natl Acad. Sci. USA* **118**, e2109729118. (doi:10.1073/pnas.2109729118)
58. Coomer MA, Ham L, Stumpf MP. 2021 Noise distorts the epigenetic landscape and shapes cell-fate decisions. *Cell Syst.* **13**, 83–102. (doi:10.1016/j.cels.2021.09.002)
59. Karig D, Martini KM, Lu T, DeLateur NA, Goldenfeld N, Weiss R. 2018 Stochastic Turing patterns in a synthetic bacterial population. *Proc. Natl Acad. Sci. USA* **115**, 6572–6577. (doi:10.1073/pnas.1720770115)
60. Michailidi MR, Hadjivasiliou Z, Aguilar-Hidalgo D, Basagiannis D, Seum C, Dubois M, Jülicher F, Gonzalez-Gaitan M. 2021 Morphogen gradient scaling by recycling of intracellular Dpp. *Nature* **602**, 287–293. (doi:10.1038/s41586-021-04346-w)
61. di Pietro F *et al.* 2021 Rapid and robust optogenetic control of gene expression in *Drosophila*. *Dev. Cell* **56**, 3393–3404. (doi:10.1016/j.devcel.2021.11.016)
62. Hofer M, Lutolf MP. 2021 Engineering organoids. *Nat. Rev. Mater.* **6**, 402–420. (doi:10.1038/s41578-021-00279-y)
63. Dalwadi MP, Pearce P. 2023 Universal dynamics of biological pattern formation in spatio-temporal morphogen variations. Figshare. (doi:10.6084/m9.figshare.c.6463359)